POLITECNICO DI TORINO

Master's Degree in Biomedical Engineering

3D-printed DNA-responsive hydrogels

Supervisor:
Dr. Ignazio ROPPOLO

Co-supervisor:
Dr. Francesca FRASCELLA

Candidate:
Cristiana DRAGO s302390

Academic Year: 2023-2024

ABSTRACT

During the last decades, the tendency of designing and developing smart materials has skyrocketed in a multitude of fields, especially in those where interaction with biological systems is researched, e.g. **soft robotics**. In this context, **supramolecular hydrogels** have attracted a great deal of interest because of their ability to respond to diverse external triggers while maintaining elasticity and a soft texture.

Even if **DNA** is well-known for being the most precious molecule within living organisms as it holds the secret of life, it is still a biopolymer and can be included in stimuli-responsive hydrogels. This offers numerous advantages because hydrogen bonds between base pairs of complementary DNA strands produce a highly specific and reversible response.

The purpose of this experimental thesis was to engineer a **DNA-based hydrogel** and drive its expansion by the mechanism of the **hybridization chain reaction**. This microscale process involves cascading interactions between DNA strands belonging to the hydrogel and complementary ssDNA dissolved in an expansion buffer.

To better appreciate on a macroscopic scale the increment in dimensions, millimetric samples should be created. Hence, **3D printing** through digital-light processing (**DLP**) technology has been chosen as the most convenient fabrication method. Indeed, DLP printers can rapidly produce tridimensional objects by photopolymerizing liquid resins a layer at a time with the resolution in the order of micrometers, that is the dimension of each light source's pixel. Considering all the additive manufacturing techniques for processing hydrogels, DLP can guarantee smaller features and higher geometric complexity than the others.

Therefore, the thesis work developed in four main phases.
During the first one, a preliminary study on the **resin composition** was carried out by comparing different photo-initiators and monomeric units. Thanks to optical spectroscopical analysis and photorheological tests, a combination between PEGDA and PEGMEMA in 2:1 proportion initiated by LAP seemed to have the ideal performances to be part of the DNA-based hydrogel.
In a second step, the optimal **printing parameters** had to be looked for and, once achieved, printing resolution has been challenged by fabricating smaller hydrogels with more **complex geometry**. Furthermore, a **multi-material printing** has been tented to fully

exploit the potential of the employed device.
After demonstrating the possibility of successful 3D printing even with ultra-low amount of resin (less than 20 µL), the third phase of the work was faced: the validation of the **DNA-driven expansion process**. A swelling protocol was set up and the samples' volumetric expansion was visually monitored by calculating the increment of the surface area with the help of MATLAB tools.
The fourth part of the experience focused, instead, in verifying the **specificity** of the process.

The obtained results were remarkably positive: the surface of samples containing DNA increased by approximately 15%, while negative control samples, namely similar hydrogels lacking in DNA, did not expand. Specificity was proven by swelling samples in an expansion buffer that contained not complementary hairpins and, as expected, initial dimensions were maintained.

The experimental outcomes of this thesis work have proved the compatibility of the DNA-driven expansion process with an innovative fabrication method and have paved the way for future developments with more challenging compounds such as RNA or nucleotides expressed by leaving systems.

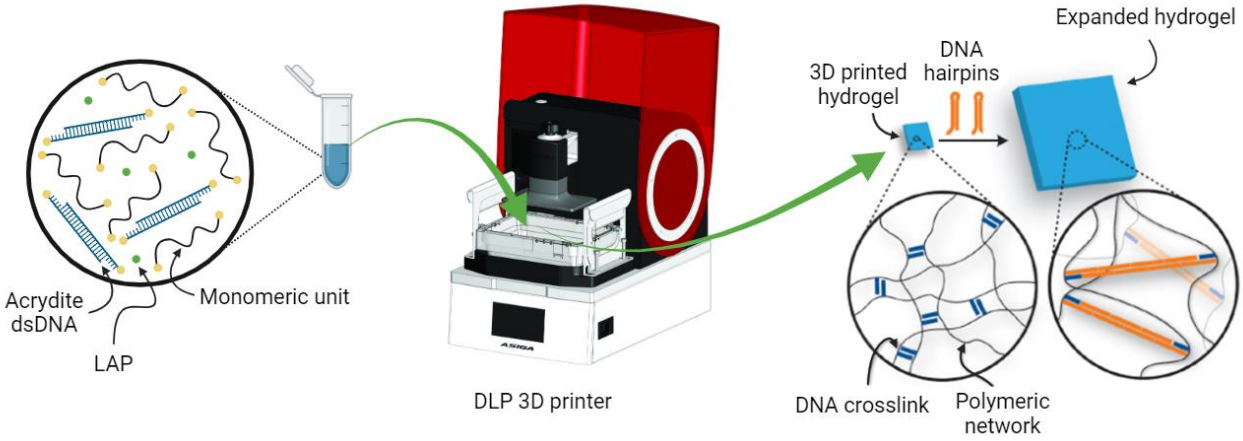

Figure 1 Graphical abstract

SUMMARY

1 HYDROGELS

Among the large variety of functional materials, **hydrogels** are some of the most employed ones. Thanks to their peculiarities, they have been used for over a century in different fields. However, only in the last decades they took a step forward in the biomedical sector because of the slow evolution of knowledge on polymers' biocompatibility (1).

As etymology could suggest, according to the IUPAC definition, they are colloidal three-dimensional structures swollen by water (2), composed of a solid, usually polymeric, and a liquid part. The solid polymeric network must trap a huge amount of water during its formation and then retain it. Consequently, **polymers** employed in the synthesis of a hydrogel must be hydrophilic, but also sufficiently stable to maintain a macromolecular structure.

The desired characteristics of the final object drive the materials' selection and design according to the final purpose and the intrinsic characteristics of the element used. For instance, biocompatibility and cytocompatibility are required in most of the biomedical applications, and consequently the elements of the hydrogels should be defined to fulfill this aim. Alternatively, biomimetic mechanical properties or biodegradability can be required, and this employ a further design of the material. The wide range of polymeric materials available and the possibility to easily tune their properties perfectly match those requirements.

In fact, polymers are macromolecules made up of smaller units stacked together, called monomers, which are responsible for the properties of the entire molecule. Polymers can be classified as **copolymers**, if two or more types of monomeric units link together, or **homopolymer** otherwise. The advantage of copolymers is that they can be engineered to show two different properties, as amphiphilic polymers.

According to their origin, polymeric materials can be classified in natural or synthetic ones. In general, **natural polymers** have animal origin, nevertheless there are some coming from plants. For instance, gelatin or collagen can be extracted from bovine and swine sources, whereas alginate from seaweeds. They are manifestly biocompatible and hydrophilic because of their natural occurrence in the extra-cellular matrix of tissues, which is a water-based environment. Most of them are biodegradable too, meaning that they can be degraded by enzymes or microorganisms (3). However, their mechanical properties are

relatively low and may change from batch to batch since their production depends on the environment and various physical factors (4). So, the properties of hydrogels based on natural polymers, e.g. the mechanical properties or the swelling ability, can have certain variability.

Alternatively, hydrogels can be synthesized starting from **synthetic polymers**. Being obtained from well-defined chemical procedures, those have defined chain length and chemical structure. A good example of this versatility are polyurethanes (PUs), that are made up of a combination of monomeric units in which a macro-diol, a diisocyanate and a chain extender are linked together. Depending on the choice of these, particularly of the chain extenders, PUs can give birth to very dissimilar, even opposite materials: from soft and flexible to rigid and hard ones. A good strategy in the biomedical field is to include a chain extender that can be deteriorated by enzymes in order to make all the PU biodegradable (5). Some other perks of synthetic polymers compared to natural are higher mechanical resistance and lower price. Although a discrete quantity is biocompatible, such as polyethylene glycol (PEG), polycaprolactone (PCL) and polyacrylamide (PAA), cells cannot adhere to the polymeric surface of most of these materials because they do not show functional groups recognizable by cell membrane receptors, e.g. integrins. Thus, a **hybrid solution** is generally preferred (6): different strategies exist to functionalize synthetic polymers with natural ones and include them in the same hydrogel. In this way the final material benefits from the advantages of both types.

1.1 SYNTHESIS OF HYDROGELS

The hydrogel preparation consists of a sol-gel transition, in which **pre-polymers**, also called **oligomer chains** or **monomeric units**, firstly dispersed in water (or in a water-based solvent), crosslink together jellifying the solution. Hydrogels can be classified into two types depending on the nature of the crosslinks (7):

- Permanent hydrogels
- Supramolecular hydrogels

This distinction is fundamental because their synthesis depends on it.

1.1.1 Synthesis of permanent hydrogels

In **permanent hydrogels**, also called **chemical hydrogels**, pre-polymers establish strong intermolecular covalent bonds, so the synthesis of their network consists in very similar reactions to the ones occurring during the formation of a single polymer:

- Step-growth polymerization
- Chain-growth polymerization

Pre-polymers who undergo a **step-growth polymerization** have functional groups on both the extremities that can spontaneously react with the crosslinking agent's ones. So, when they're both added to the solution, the reaction self catalyzes, which means that it doesn't require an initiator. The presence of two reactive endings has an interesting effect on the reaction kinetics because the crosslinked chain length grows with an exponential trend. Initial monomeric units tend swiftly to disappear in favor of intermediate products that have the same functional endings and, even when the reaction is completed, the final product contains active endings that potentially could still react if additional crosslinkers are added.

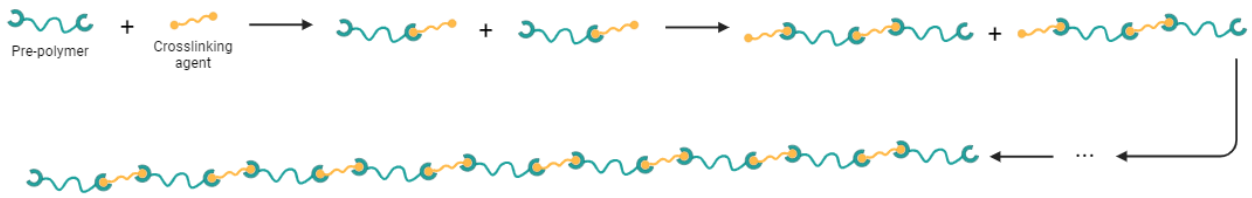

Figure 2 Schematic representation of step-growth polymerization

For instance, polyurethane-based hydrogels (see Figure 3 (8)) are fabricated with this technique and the reaction between chains is usually a condensation with the emission of little molecules of water.

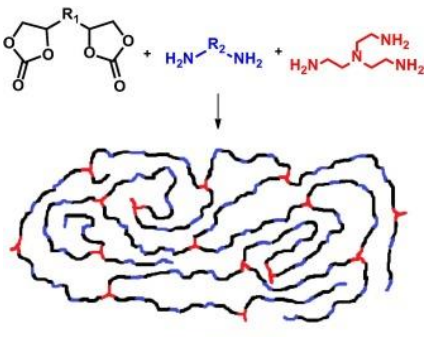

Figure 3 Example of synthesis of a PU-based hydrogel.

Whereas generally **chain-growth polymerization** is an addition reaction that always needs an initiator. This interacts with pre-polymers when activated and enable the beginning of the reaction. Compared to the forementioned process, this time pre-polymers have only one active ending at a time and chain growth linearly. The mechanism consists of three phases: initiation, propagation and termination.
During the initial phase, the initiator is activated by some factors, such as UV light, heat or a chemical factor, and an unstable site is generated, for example a radical or an ion or an organometallic complex (9). This is so unstable that spontaneously interacts with one ending of the pre-polymer and bond to it. Then, it is transmitted to the other end of the pre-polymer that in turn reacts with another one and the reaction progresses in this way. Termination occurs only when two intermediate products link together and the entire molecule is stabilized.

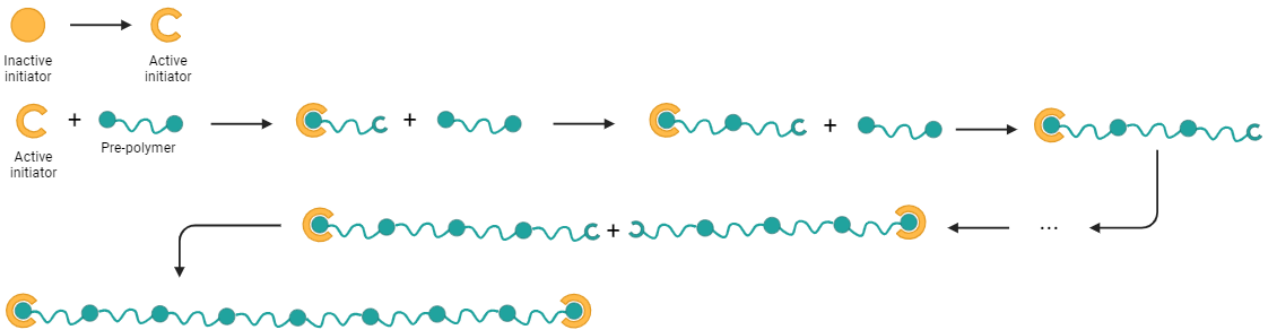

Figure 4 Schematic representation of chain-growth polymerization

The most common reaction is the **free radical polymerization** and, in greater detail, **photopolymerization** where the initiator is activated by visible or UV light. All the pre-polymers with acrylic endings, as PEGDA or PAA, are good candidates to form hydrogels in this way.

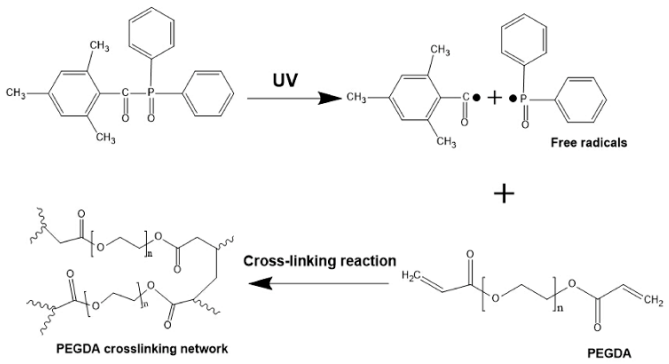

Figure 5 Example of synthesis of a PEGDA-based hydrogel.

A similar crosslinking method is the **gamma and electron beam polymerization** that induces the formation of radical directly onto the pre-polymeric chain thanks to high energy radiations (10). This mechanism implies the same three phases of the free radical polymerization but avoiding the use of an initiator.

For biomedical purposes, other niche methods exist, such as the **crosslinking via enzymes** (10). For instance, transglutaminases are Ca^{2+}-dependent enzymes used to cross-link PEG hydrogels in the presence of lysine copolymers (11). It has been shown that they are good candidates to create triggered injectable hydrogels to deliver bioactive substances *in situ* (12).

1.1.2 Synthesis of supramolecular hydrogels

Supramolecular hydrogels are also called **reversible** or **physical hydrogels** because of their ability to establish weak reversible non-covalent bonds between pre-polymers.
They have two main advantages on permanent hydrogels: there is no need for a chemical initiator, which usually is cytotoxic, and they can be triggered by external stimuli, so that they can be precisely engineered to respond only at specific conditions.

The most common synthesis method is based on **ionic interactions** between pre-polymers and mono- or divalent ions. For instance, alginate-based solutions can jellify at mild conditions in the presence of Ca^{2+} ions. These replace Na^{+} ions of glucuronic acid molecules belonging to two different alginate chains by linking them together in a “egg-box” junction, named after the particular shape (13).

The powerful of this technique is that, in some cases, it is applicable to polymers that don’t show any ionic binding sites, e.g. dextran (14).

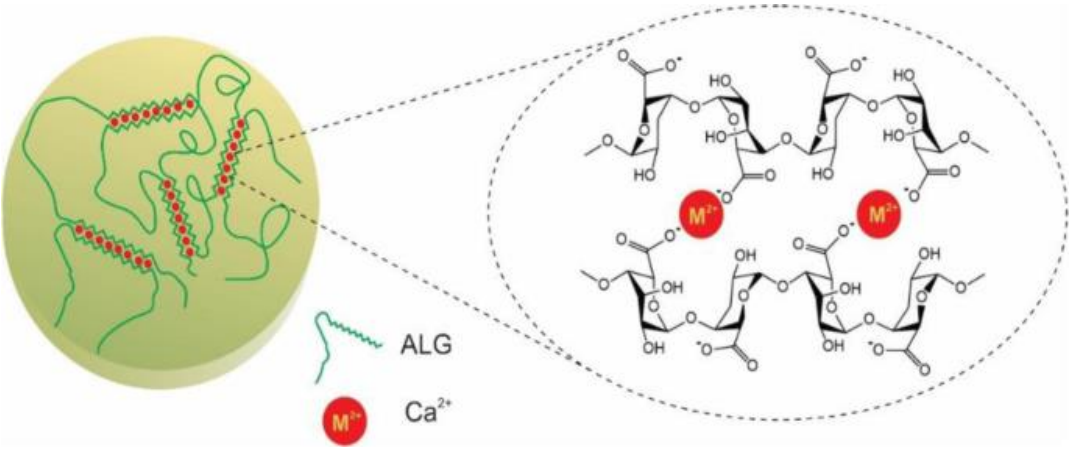

Figure 6 Example of synthesis of an alginate-based hydrogel.

Some other valid strategies engage **hydrogen bonds** (H-bonds) whose dynamic nature provides good flexibility to the hydrogel (15,16), **crystallization** through freezing-thawing cycles (10,17) and **stereocomplex formation** by crosslinking molecules of opposite chirality, e.g. for the polylactic acid (PLA): PLLA and PDLA (7,10).

1.2 APPLICATIONS

Even though hydrogels are well known for being applicable in many contexts thanks to the versatility of their characteristics, only some biomedical applications will be highlighted in this thesis work.

***In vitro* modeling of three-dimensional human tissues** is one of the main applications because hydrogels' mechanical resistance is compliant to soft tissues, in the range of 1-100 kPa (18). Scientists have been developing either healthy or pathological models for diverse purposes that basically have the same origin: reduce and, when possible, avoid animal experimentation since it is unethical and not really viable. **Pathological models** could be useful to investigate mechanisms involved in the onset of a disease in a simpler environment than a living one or to test new potential drugs to treat it (19). One of the possible uses of the **healthy models**, instead, is in the cosmetics industry to test the biocompatibility and the efficacy of new make up or skin care products before commercialization (20).

Alternatively, hydrogels could be directly brought in contact with the human body for ***in vivo* applications**. Nowadays, for instance, silicone-based hydrogels are one of the most prescribed soft **contact lenses** on the market (21), born to overcome the lack of oxygen permeability in PMMA lenses which caused evident irritation problems in the cornea. Besides this advantage, hydrogel's transparency and the modulation of its thickness allow to correct eyesight defects. Another interesting application is the treatment of **wounds** thanks to hydrogel-based **dressings**, which seems to be the most promising approach (22). A proper materials' choice provides a suitable environment for skin regeneration, allowing body cells to swiftly colonize the hydrogel and producing new healthy tissue. A good common practice is to charge the hydrogel with growth factors to speed up the regenerative process. Moreover, commercialized hydrogels for wound healing have anti-bacterial and anti-inflammation properties that surely improve the procedure.

However, among the most recent applications, **soft robots** are particularly noteworthy because they tackle the limitations of conventional robots, too rigid to interact with human body and very little flexible (23). Soft robots are made up of hydrogels finely designed in shape and composition to act like rigid-bodied robots but with more advantages. Mechanically speaking, hydrogels have relatively low elastic modulus and can endure up to 1000% of mechanical strain (24), while water content allows the hydrogel to be transparent, so that it can transmit optical information, and conductive thanks to the ions dissolved in it. Moreover, the ability to encapsule any additive bigger than the dimension of the polymeric meshes, gives the hydrogel specific features. These are the reasons why hydrogels are perfectly suitable for at least five components of a soft robot; they can serve as actuators, sensors, communicators, power sources and even as computational circuits. Take, for example, a thermally responsive **soft actuator** based on two stacked layers of different hydrogels (23,25). When temperature raises, the layer with lower critical solution temperature swells, while the other one shrinks due to the upper critical solution temperature (Figure 7-a, (23,25)). In this way it is possible to fabricate a gripper that can grasp little objects when in contact with hot surfaces (Figure 7-b, (23,25)).

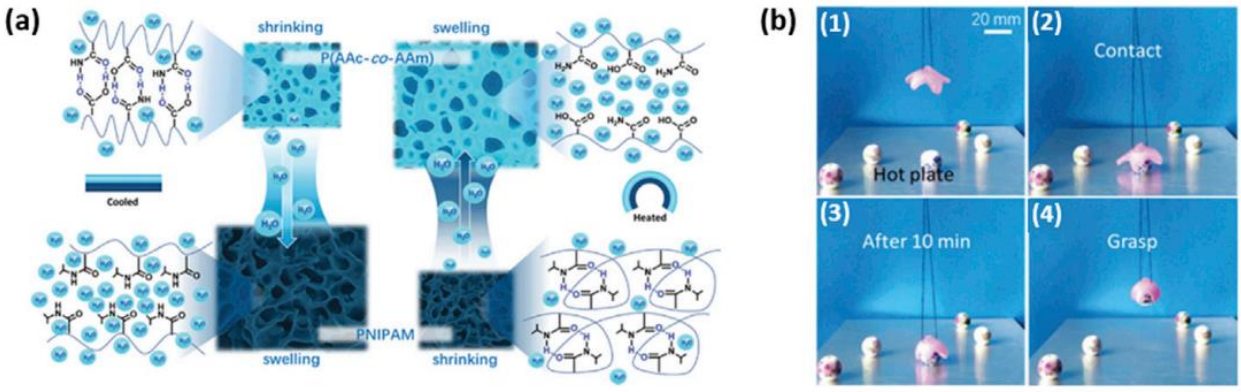

Figure 7 (a) Scheme of the mechanism of thermal responsiveness of a soft actuator (b) Thermally responsive soft gripper.

1.3 DNA-BASED HYDROGELS

1.3.1 DNA structures

Every kind of unicellular or multicellular living organism contains a fundamental biomolecule called **deoxyribonucleic acid** (**DNA**), whose main function is to store the genetic information that makes unique every single creature. The smell of flowers, the color of animal fur, the parent-offsprings resemblance, the specific microbial activity, everything is written into the genetic code within the DNA structure. For this reason, it is extremely valuable and it needs to be protected. The discovery of the DNA molecule arrangement is relatively recent and dates back to 1953, thanks to the remarkable contribute of Dr. James Watson and Dr. Francis Crick (26) which granted them the Nobel prize in 1962. The two scientists found out that the secret of life is contained in a double-stranded helix organized in piled monomeric units called **nucleotides**. Each one is constituted by three groups: a sugar, the deoxyribose, a phosphate group and a nitrogenous base, namely adenine, thymine, cytosine and guanine. The first two compose the backbone of each strand, while hydrogen bonding between bases sticks the two filaments together: specifically adenine links to thymine through two H-bonds, while cytosine to guanine through three (27).

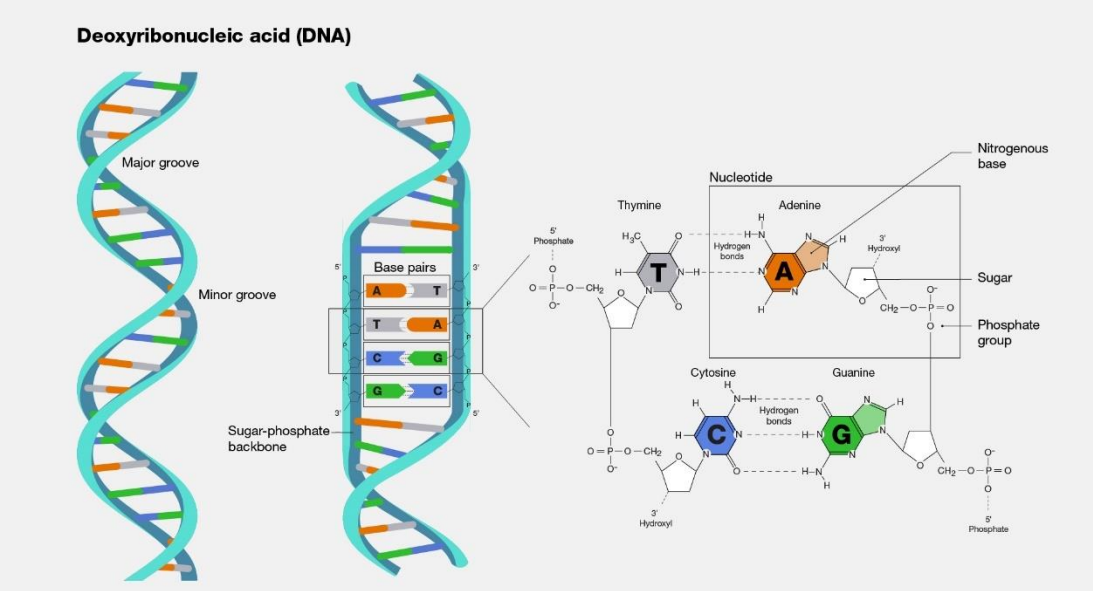

Figure 8 DNA structure

Nevertheless, it has been found out that DNA base sequence has a cardinal role not only in coding genetic information. Experimental evidence suggested the existence, under physiological conditions, of alternative sequence-dictated DNA structures, that can interact with proteins and have an implication in human diseases (28). For instance, **G-quadruplexes** are guanine-rich sequences binding in tetrads that have part in cancer development and cells' malignant transformation (29). Likewise, **i-motif** structures can form in oncogenes if sequences are rich in cytosine (30). **Aptamers**, instead, are cruciform ssDNA molecules whose specific function is similar to antibodies, i.e. to recognize low molecular-weight targets (31,32).

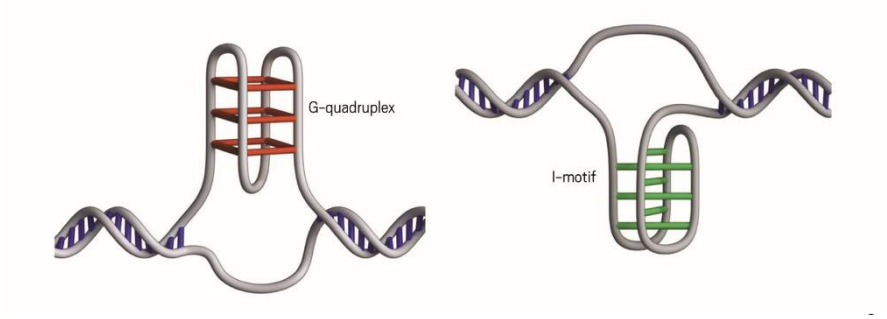

Figure 10 G-quadruplex and i-motif DNA structures.

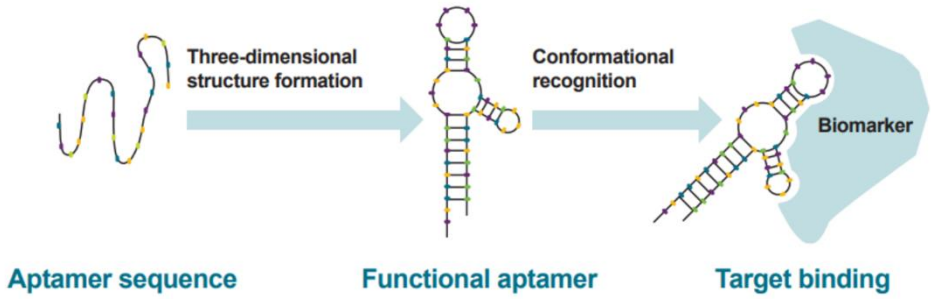

Figure 10 Structure and function of aptamers.

1.3.2 DNA-based hydrogels

These extraordinary breakthroughs on sequence-dictated DNA structures with alternative functions reshaped the concept of DNA as a functional material, opening new avenues for its applications. In 1982, Dr. Nadrian Seeman was the first to use DNA for not-genetical purposes, giving birth to the field of **DNA nanotechnology** (33). The main goal of this branch is to design nanostructures using artificial short nucleic acids for technological purposes by exploiting their peculiar biochemical properties. In recent years, thanks to the rapid evolution of knowledge about this subject, both static, e.g. DNA nanotubes (34), and functional structures have been developed. In 1994, the mathematician Dr. Leonard

Adleman carried out computations at the molecular level by using standard protocols of molecular biology and enzymes to manipulate DNA (35). This was the beginning of the development of **DNA computer** and **DNA-based computational circuits** (36,37), a cutting-edge research field that is interesting a growing number of scientists. While, in 1996, DNA was used as a component of a chemical hydrogel to make it responsive to external stimuli (38). The early-designed base sequence and the weakness of H-bonds confer high specificity and reversibility to **DNA-based hydrogels**. For this reason, they too are progressively getting the attention of scientists, who have elaborated two types of them: pure and hybrid.

Pure hydrogels are obtained by the mere crosslinking of small DNA molecules organized in structures that have one central junction and more than two endings, generally called nanostars (as in Figure 11 (39)). Different strategies are used to bind endings, e.g. hybridization of sticky ends, formation of i-motifs or enzymatic ligation (40).

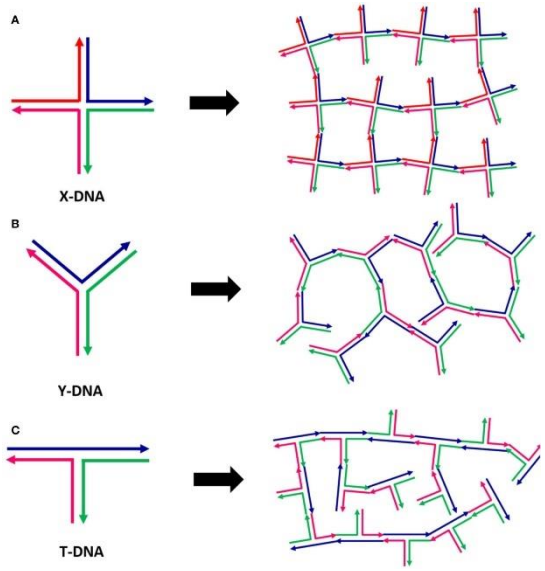

Figure 11 Examples of pure DNA-based hydrogels with different monomeric unit' shapes: X-DNA (a), Y-DNA (b), T-DNA (c).

Alternatively, **hybrid hydrogels** are formed by the copolymerization of DNA molecules with other polymers. As every kind of combined materials, they benefit from the perks of both elements, resulting in a well-controlled multi-responsive gel.
Whereas DNA effects have already been widely discussed, the polymeric contribution is manifested by their chemical stability, flexibility and ease to handle (40). One of the most common strategies is to create a polymeric backbone by photopolymerizing molecules with acrylic endings and functionalize them with acrydite-modified DNA (41). In this way,

the entire structure is stable and permanent, but can still be triggered by external physical and chemical stimuli thanks to the presence of DNA.

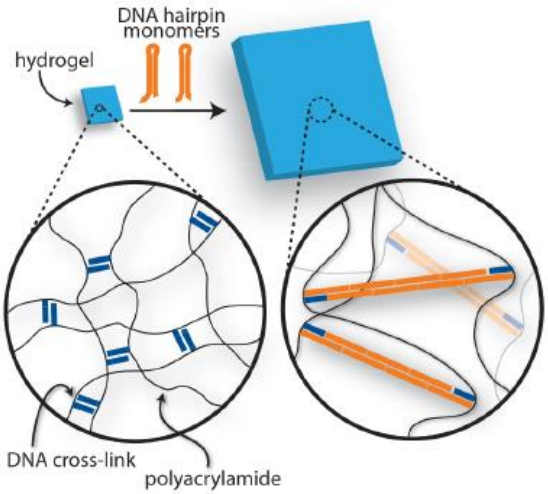

Figure 12 Example of hybrid DNA hydrogel triggered by complementary hairpins.

1.3.3 DNA response to external stimuli

DNA is an exceptional candidate for the engineering of smart materials thanks to its ability to respond to a wide range of stimuli. Over the last decades, scientists have addressed their efforts to design DNA-based responsive hydrogels attempting both physical and chemical approaches as triggers (42).

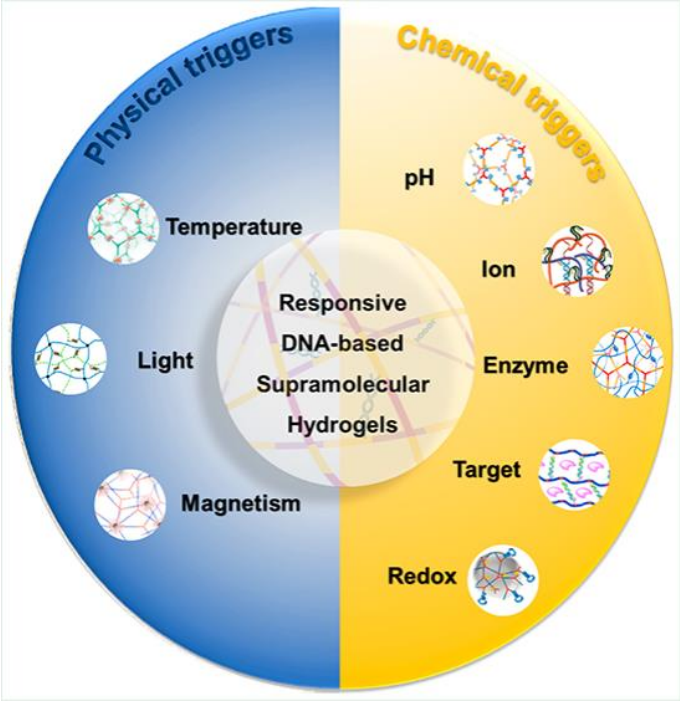

Figure 13 Overview of the main external triggers for DNA-based hydrogels.

All these methods have in common the purpose of changing the hydrogel mechanical behavior by altering the DNA structural organization.

For instance, **temperature adjustment** is one of the easiest and common strategies in many molecular biology techniques to pair or unpair two DNA strands. Thus, in 1996 Dr. Nagahara and Dr. Matsuda created the first DNA-based hydrogel and subjected it to high temperature (38). That way, they induced a reversible transition from the gel state at room temperature to solution at higher temperatures.

About this matter, **pH variation** also produced noteworthy results. In 2009, Cheng *et al.* first proposed a pure DNA-based hydrogels with pH-responsiveness (16,42). The gel formation consisted in Y-shaped triplets of DNA linking together through the formation of i-motifs at the binding edges when pH was sufficiently acid. However, at higher pH values, the i-motif structures broke apart leading to a reversible transition to sol state.

Willner *et al.* proved that the same reaction could occur by means of **metal ions** too (43). They created a polyacrylamide-DNA hydrogel whose DNA sequence where complementary except for some cytosine-cytosine mismatch that did not allow the binding between strands, so hydrogel was in a solution state. When Ag^+ ions were added, C-Ag^+-C bridges were formed causing its jellification. They verified the reversibility of the process by the addition of a counter-trigger. In fact, cysteamine can combine to Ag^+ ions and break the previous complex, reverting the hydrogel to a liquid state.

In addition to the examples already mentioned, DNA can also be triggered by **UV light**. Kandatsu *et al.* proposed the employment of an artificial base (^{cnv}K) to produce a repetitive gel-sol transition by the reversible hybridization of sticky ends containing that base (44). Wheter irradiated with 366 nm UV light, ^{cnv}K can react with thymine hybridizing two strands of DNA, while at 340 nm the two bases dissociate.

Actually, in terms of triggered effects, not only a sol-gel transition but a wide range of outcomes can be engineered according to the goal of the research. For instance, the research group lead by Gracias has developed a DNA-based hydrogel responding to the addition of **nucleic acidic fuel** with a volumetric expansion (41,45).
The molecular mechanism on which this process is based is called **hybridization chain reaction** (HCR) and requires a DNA-based hydrogel (containing C-C' dsDNA) and an expansion buffer solution containing two oligonucleotidic DNA strands organized in hairpins (H_1 and H_2).

Figure 14 (41) provides information about how this spontaneous process works. The two DNA hybridized strands contained in the hydrogel are not totally complementary. The exceeding single stranded sequence is a promoter for the beginning of the reaction; indeed, it is complementary to the H_1 hairpin who unfolds and joins the chain because of the thermodynamic affinity. H_1 hybridizes to both C and C' strands but still contains a binding site for the H_2 hairpins. At this point, H_2 acts exactly as H_1 and once again joins the chain. The process keeps going until no more hairpins are available for the cross-hybridization. The last free binding site is still active so the cross-expansion of the chain potentially can grow with the addition of further hairpins; that's why they are called nucleic acidic fuel.

This elongation of the DNA chains thanks to hairpins translates into a dimension variation on a macroscopic scale.

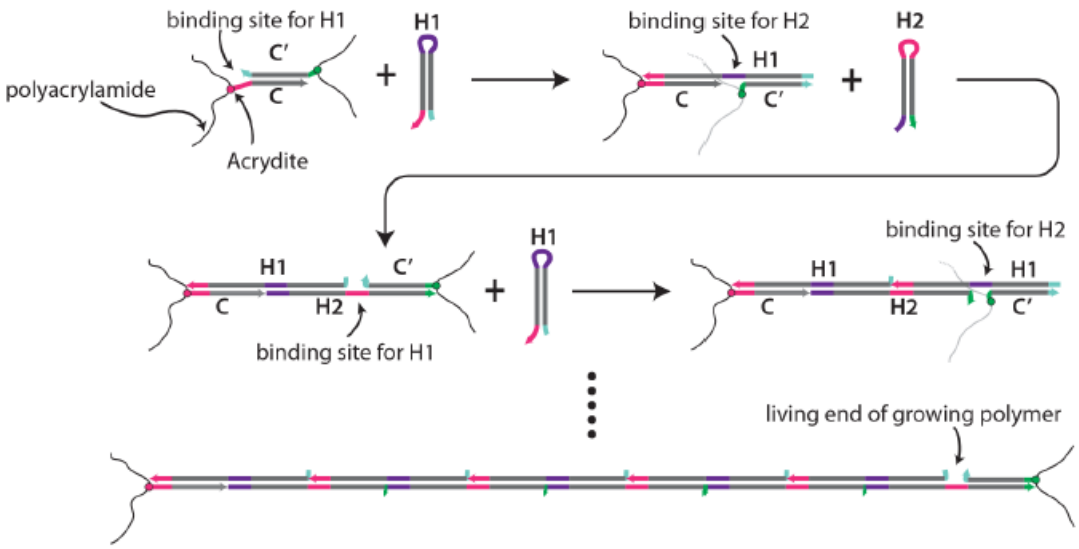

Figure 14 Hybridization chain reaction (HCR) process.

In this thesis work, this latter was the preferred method to trigger a DNA-based hydrogel. Therefore, the planification of the entire experience took inspiration by Gracias *et al.*'s works.

2 ADDITIVE MANUFACTURING

For centuries, human craftsmanship and industrial production relied predominantly on **subtractive manufacturing** techniques. These traditional methods, such as turning, milling or drilling, involve the removal of material from a larger block to achieve the desired shape.
Nowadays, they exploit computerized numerical control (**CNC**) **machines** that provide higher precision and resolution, besides time-saving processes, with respect to former manual approaches (46). However, despite their effectiveness, subtractive techniques often result in significant material waste and can be limited in their ability to create complex geometries.

To overcome these drawbacks, in 1986 stereolithography (SLA), the first **additive manufacturing** (**AM**) technique, was patented by Charles Hull (47) and, ever since, has revolutionized the way we approach fabrication. According to the ISO/ASTM 52900 standard, AM is defined as “the process of joining materials to make parts from 3D model data, usually layer upon layer, as opposed to subtractive manufacturing and formative manufacturing methodologies” (48).
Indeed, in contrast to the aforementioned methods, additive manufacturing builds objects through the addition of material precisely where it is needed.
It is also improperly known as **rapid prototyping** because, in its early stage, it used to be employed to swiftly develop prototypes aimed at enhancing the efficiency of the industrial process. Yet, over time, a shift to full-scale production has been observed and has significantly impacted various sectors: from automotive to building (49).
Likewise, sometimes additive manufacturing can be mixed up with **3D printing**. This last normally refers to a huge sub-category of AM in which objects are produced layer-by-layer. For this reason, the ISO definition specifies “usually layer upon layer” even if it is not always the case; take, for example, the CNC accumulation method (50). Furthermore, 3D printing is associated with more recreational and home-made applications; whereas additive manufacturing to industrial large-scale processing (51).

2.1 AM WORKFLOW

The AM workflow is a comprehensive sequence of steps that transform a digital design into a material object. Understanding this workflow is crucial for optimizing efficiency and achieving high-quality results. The process encompasses eight key stages, resumed in Figure 15 (49), each contributing to the final outcome.

1. **CAD modelling**: firstly, a 3D model of the desired object is digitally realized through one of the CAD software available on the market. The drawing can be entirely computer-designed or can come from a 3D scanning of an existing object, performing what's known as reverse engineering.
2. **STL file**: the CAD is then converted to the "Standard Tessellation Language" (STL) file format, which has been invented by Charles Hull (52), the father of additive manufacturing, and that has become an industrial standard. This format approximates surfaces with polygonal, generally triangular, meshes who define the resolution of the printed object. The more and little triangles have been generated, the more the final product will be resolved.
3. **Data preparation**: a slicing software is responsible for traducing information contained in the STL file into the "G-code", namely a sequence of commands containing printing instructions. Both basic and advanced parameters can be manipulated thanks to the G-code: not only the object size, location and orientation but also number of layers in which it is sliced, layer thickness, printing time, energy intensity, temperature and so on.
4. **Machine set-up**: before the real printing phase, the correct configuration of the printing device must be assured. Thus, a preliminary calibration should be performed.
5. **Built**: the part-building process is totally automated, and the printing machine works autonomously following the G-code instructions. At the end of this phase, the material object is created.
6. **Support removal**: products with complex geometries, such as hollowed ones, may need supporting structures to be printed, which are then removed at the end of the printing process. Consequently, this phase implies a meticulous and skilled manipulation of samples.

7. **Post-processing**: it is very common to further treat components after their printing to remove raw material residuals and to smooth the surface texture. So, products are cleaned with specific procedures and then abraded or sintered.
8. **Application**: at the end of the process, objects are now ready for usage.

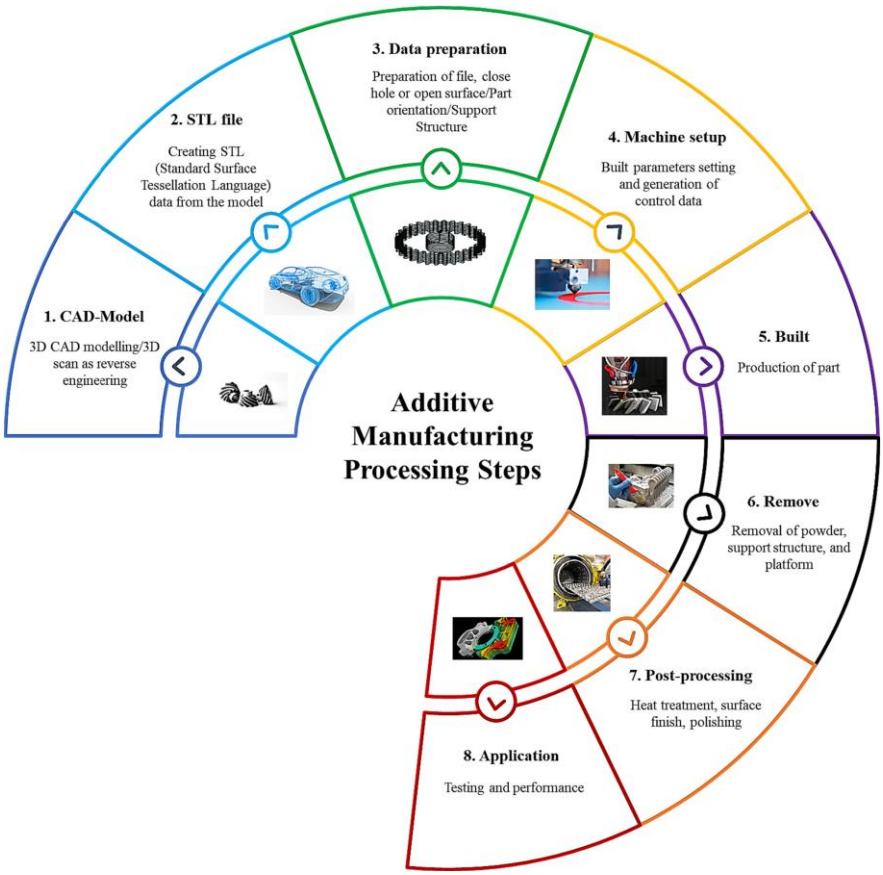

Figure 15 Additive manufacturing workflow

2.2 CLASSIFICATION OF AM PROCESSES

According to the ISO/ASTM 52900 standard (48), they exist seven categories of additive manufacturing processes; however two additional methods, cold spraying and additive friction stir deposition, have been developed in recent years (49).
To better understand their functionality, they will be briefly described below.

- **Material extrusion**: Fused deposition modeling (**FDM**) and fused filament fabrication (**FFF**) are two of the most employed techniques in 3D printing and they belong to the material extrusion family. A filament of raw material, usually a thermoplastic polymer, melts passing through a heated extruder. Then, it is selectively deposited with constant flow on a platform where it solidifies, cooling down.

Similar techniques, e.g. direct ink writing (**DIW**) (53), are based on the extrusion of a liquid ink that solidifies through the evaporation of the solvent.
During the process, the extrusion nozzle can have three degrees of freedom (moving within the x, y and z axes) or it can move only through the x-y plane and the platform will go up and down along the z-axis.
This family of techniques is very common because it is easily accessible and simple to use, besides fabricating mono- and multi-material objects with good structural properties (54).

- **Vat polymerization**: it is the first additive manufacturing technique to be invented. It is based on the polymerization of liquid photosensitive resin by the means of light at different wavelengths. The two most common methods belonging to this class are stereolithography (**SLA**) and digital light processing (**DLP**).
- **Material jetting**: this technique is the most similar to 2d inkjet printers because a nozzle discharges droplets of one or more photosensitive substances continuously or only when needed. Then, the entire layer is photopolymerized by a UV laser before proceeding with the next one. The perks involved with using this method are the printing and curing rapidity and the possibility of performing a multi-material printing (55).
- **Sheet lamination**: this technique consists of the stacking of adhesive-coated sheets and the subsequent slicing into the final form through a knife or a laser cutting. Depending on the material of which sheets are made up of, the techniques is named differently. For instance, the sheet lamination of metals is usually called ultrasonic additive manufacturing (**UAM**).
- **Powder Bed fusion**: this class of methods selectively melt and fuse powdered materials by employing a laser, such as for selective laser melting (**SLM**) and selective laser sintering (**SLS**), or an electron beam, in the case of electron beam melting (**EBM**). Normally, it is the building platform that moves downward once the layer of powder has fused. In this technique the unmelt powder is recycled, and components are fabricated with great accuracy.
- **Direct energy deposition**: this fabrication method exploits thermal energy produced by lasers, electron beams or electric arcs to melt materials while they are deposited. It is a complex process that has its origins in welding and has been used to repair or to add materials to a pre-existing object; in fact it is not very common to create a new component only using this technique.

- **Binder jetting**: this technique mainly requires two components: the material who provides mechanical resistance in powder and a liquid binder agent. A layer of liquid binding droplets is interposed between two thin layers of powder to bind them. Among the advantages of this technique there are the recycling of unbound powder and the creation of multi-colored 3D objects.
- **Cold spray AM**: it was born as a coating technique but has evolved in an AM process. It consists in spraying fine powder particles onto a substrate through a high-velocity compressed gas-stream to ensure proper adhesion and component build-up.
- **Additive friction stir deposition**: it is a new technique that mixes up the friction stir welding with additive manufacturing. Indeed, a rotating hollow tool deposits a material onto a substrate by generating frictional heat.

Figure 16 (49) depicts a graphical representation of all these AM production processes.

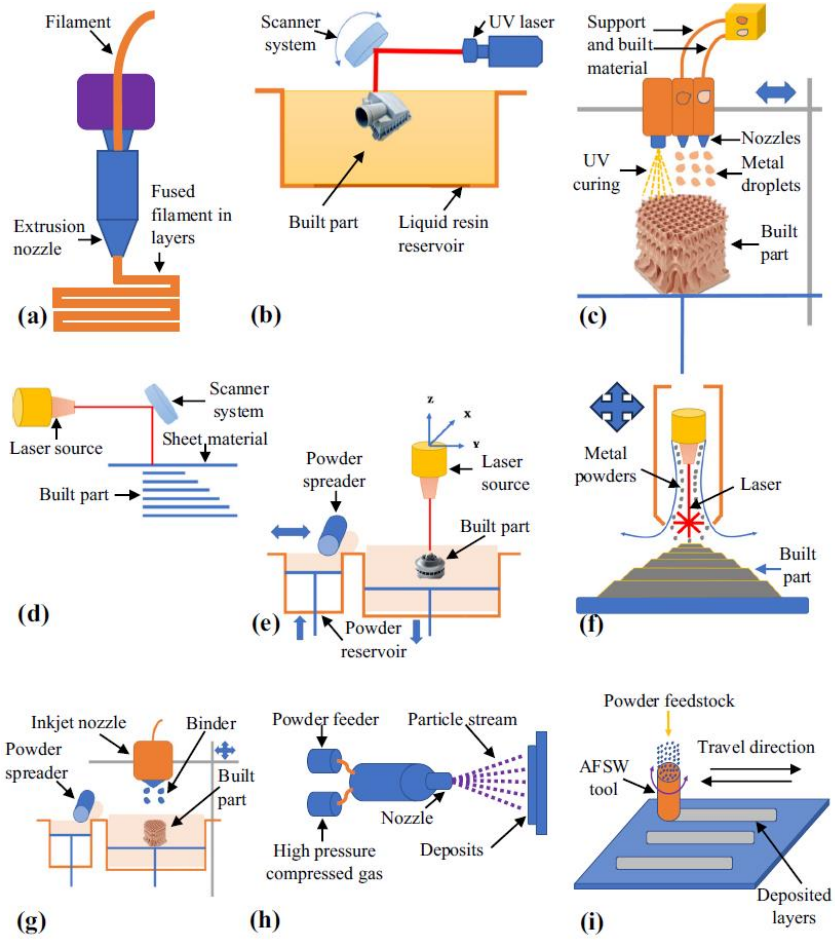

Figure 16 Graphical abstract of AM techniques: material extrusion (a), vat polymerization (b), material jetting (c), sheet lamination (d), powder bed fusion (e), direct energy deposition (f), binder jetting (g), cold spraying (h), additive friction stir deposition (i)

2.2.1 Vat polymerization

Since a VAT polymerization (VP) process will be employed during this thesis work, it will be the only one to be exposed in details.

The name of this class of techniques comes from its AM process: a liquid photocurable resin is placed into a tank, commonly known as **vat**, and it is photopolymerized by means of a controlled irradiation. For this reason, **vat polymerization** is also named **light-induced 3D** printing.

Every kind of VP is distinguished by the light source employed, nevertheless they all share the same set-up:

- A **tank** containing the **liquid resin**
- A **building platform** onto the object is built layer-by-layer
- A **mechanical actuator** that displaces the building platform along the vertical axis
- A **light source**
- The most advanced techniques have a **light mask** too

These elements can be organized into two different configurations: the top-down and the bottom-up approaches.

In the **top-down configuration** the vat is full of resin and the irradiation comes from above while the platform goes downward after each step, as in Figure 17 (b) (56). The layer is thus printed at the air-liquid interface. The main positive aspect of this configuration is the fact that the liquid resin not only serves as supply of raw material but also provides a mechanical support to the printed construct. However, it needs a significant amount of resin which will be prone to waste, the platform descent causes a mechanical perturbation of the liquid and superficial vibrations that will provoke high wait times (57) and, lastly, there is a high risk that layers will not fully polymerize due to oxidative inhibition processes (57).

Alternatively, the **bottom-up configuration** involves the laser being located below the reservoir and the platform moving upward after each step obtaining, as a consequence, an upside-down product, as in Figure 17 (a) (56). In this way all the previous drawbacks have been overcome, albeit some further clarifications should be remarked. The tank must have a transparent floor to allow the light to pass and should be coated with a silicon-based layer in order to avoid the risk of the construct sticking to it and eventually breaking. Furthermore, supports may be needed to contrast the gravity effect and the ascent of the platform must be slow enough to avoid the sample rupture (58).

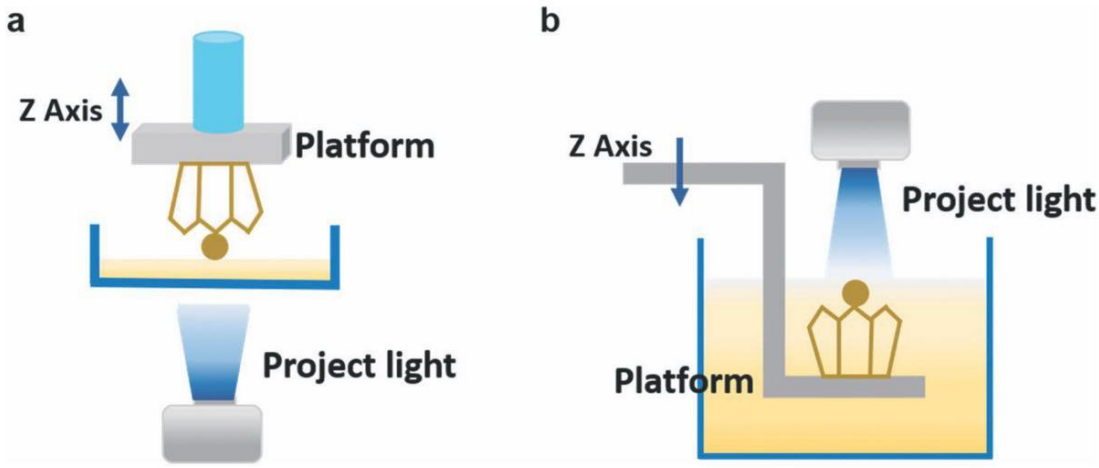

Figure 17 Bottom-up (a) and top-down (b) approaches for VP techniques.

In any case, the main parameters to control for both configurations are the light wavelength and its power intensity, the exposure time and the layer thickness. Some more advanced parameters can be adjusted too depending on the specific situation.

Regarding the **light source**, instead, devices based on **SLA**, the first VP process, have a galvanometric head that propels a **"single-point" laser beam** along the platform (x-y plane), according to the G-code commands (59). Classic SLA technology can achieve 10 µm resolution on the x-y plane (60), however the earlier micro-stereolithography (**µSLA**) has been developed to project a laser spot size of 5 µm (61).

On the other hand, **DLP** printers project UV or visible light through a digital light projector called **digital mirror device** (**DMD**). Thanks to this technology, each micro-mirror represents a pixel and can be independently oriented with respect to the others.
Unlike SLA, DLP allows the simultaneous irradiation of many mirrors resulting in the printing of the entire cross-section of the object at the same time (59). The benefits

provided by this technology have been numerous: higher printing speed, high resolution (in the order of 1 μm) and low cost (56,62).

In recent years, some more sophisticated vat fabrication methods have appeared. Take, for example, the **continuous liquid interface production** (**CLIP**) with its “layer-less” printing and the **computed axial lithography** (**CAL**), a volumetric 3D printing that generate a three-dimensional hologram; both aimed to keep improving the printing rapidity while saving a micrometric resolution (59).

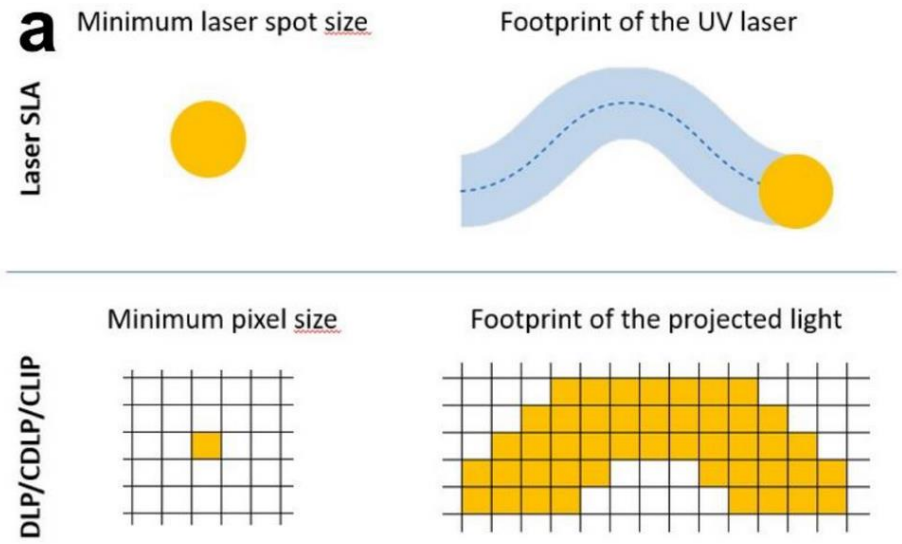

Figure 18 Photopolymerization mechanisms for different VP: SLA (up) and DLP (down).

2.2.1.1 Composition of a photocurable formulation

To fully grasp the functionality and application of photocurable resins, it is essential to delve into their composition. This section will provide a detailed analysis of the key components that constitute a typical photocurable resin, highlighting their roles and interactions (59).

PRE-POLYMER

Pre-polymers are also called **monomeric units** or **oligomers** and constitute the most abundant solute of a photocurable resin.
Pre-polymers subjected to photo-polymerization must have reactive functional groups that allow them to cross-link through a **chain-reaction polymerization**. Among all, the most suitable polymers for VP are **acrylates**, **acrylamides** and the ones containing **epoxide rings**. The first two categories undergo radical polymerization, while epoxides cationic one.

A few examples are reported here (59):

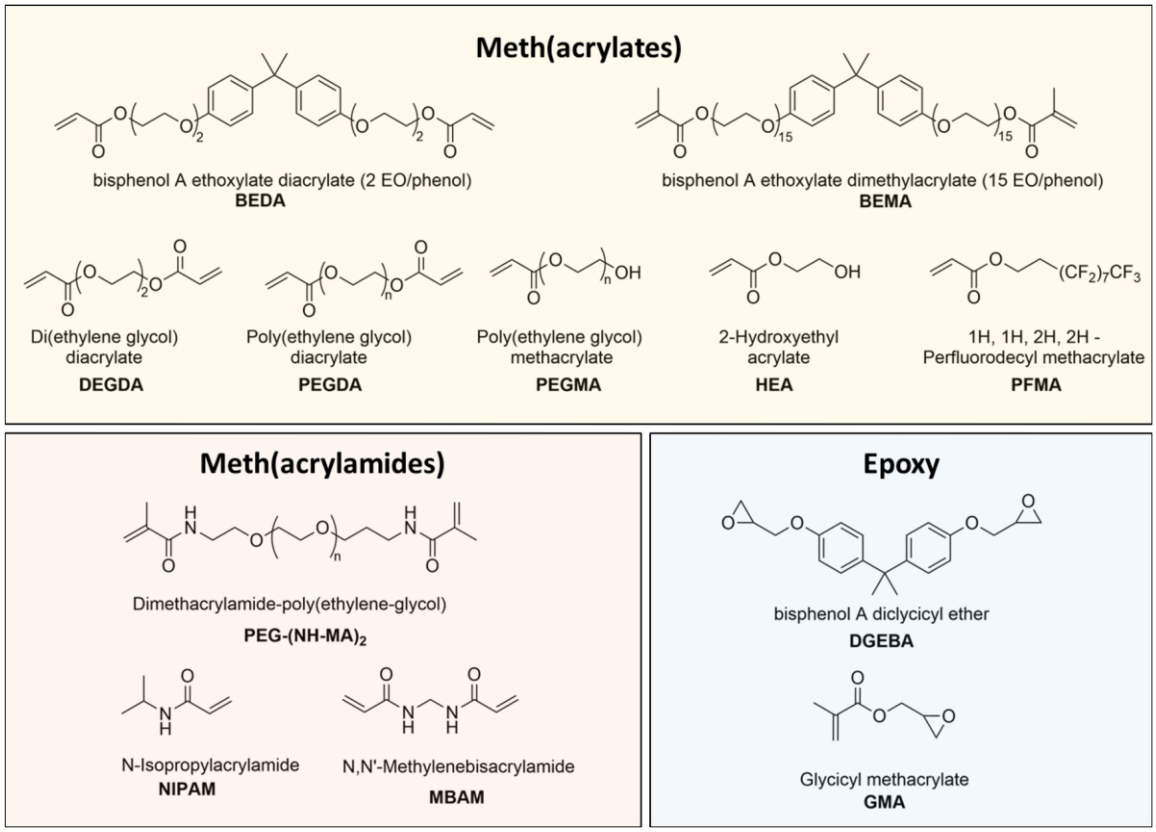

Figure 19 Most common pre-polymers for vat polymerization.

Whereas the polymeric backbone influences the mechanical and physical-chemical properties, their functional groups the reaction kinetics. For this reason, they should be carefully chosen.

PHOTO-INITIATOR

Photo-initiators are little photoreactive molecules required to begin the polymerization. When excited by light at a specific absorption range, they can generate **active species** (radicals or cations, depending on the type of PI).

Photo-initiators can be classified as **Norrish type 1**, if they are directly activated by light, or **Norrish type 2**, if they need a co-initiator to be activated.

In the choice of the photo-initiator there are two main critical requirements to satisfy: firstly, the **absorption range** of the PI must match the wavelength produced by the light source of the 3D printer. Secondly, it should be soluble in the resin solvent, thus an oil-soluble one should be picked for hydrophobic solvent, while a water-soluble one otherwise.

However, one of the greatest drawbacks when a hydrogel is aimed to be printed is the shortage of water-soluble photo-initiators.

The most common ones employed for the DLP printer are resumed here (63):

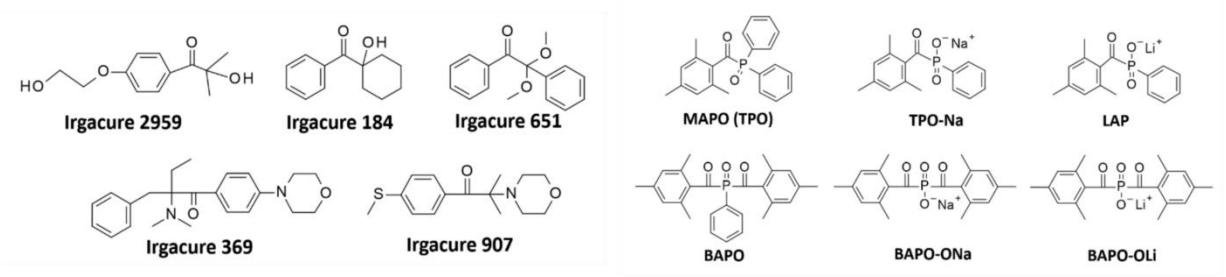

Figure 20 Common photo-initiators for vat polymerization.

PHOTO-ABSORBER

Photo-absorbers are **dye molecules** often added to photocurable resins. These can either be dispersed within the formulation or covalently bonded to the polymeric backbone of the resin. Their addition to the resin improves certain characteristics of finally printed objects, such as resolution or mechanical strength, by absorbing some of the incident radiation and thereby allowing better control over the polymerization reaction. They induce the decrease of the intensity of transmitted radiation, focusing the photon flux into a limited volumetric region. This affects both depth and breadth, helping to prevent over-crosslinking phenomena and consequently improving resolution.
The amount of dye added to the formulations is chosen based on factors such as the absorption spectrum and molar extinction coefficient, aiming to minimize competitive light absorption by other elements like photo-initiators within the formulation. While, the selection of the dye should consider the absorption spectrum of the photo-initiator and, consequently, the emission wavelength of the printer used.
The ultimate goal is to achieve a balanced resin composition that ensures **good resolution** and **rapid polymerization** (59).

FILLER

Filler molecules are added to the resin in order to create a new **composite material** with improved properties. In fact, these can endow the resin with new properties, such as electrical conductivity, rigidity or antibacterial. Fillers can have **organic** or **inorganic** origin and, usually, are available in powder form. Common materials are carbon, titanium or cellulose. Furthermore, they reduce shrinking caused by the printing process, resulting in an **increased printing accuracy** (59).

RADICAL SCAVENGER

A **radical scavenger** is a chemical substance that can remove or de-activate impurities and undesired reaction products. For instance, the most of polymeric radical scavengers are added to **avoid oxidation** of the resin or to reduce premature, spontaneous cross-linking reactions (59). More commonly, radical scavengers are used to control undesired polymerization out of irradiated areas, increasing printing accuracy.

2.3 APPLICATIONS

3D printing is revolutionizing the manufacturing landscape and is a crucial component of **Industry 4.0**. This era is characterized by the seamless integration of digital technologies and automation into production processes, and 3D printing is at the forefront of this transformation (49).

3D printing aligns perfectly with the need for **digitalization** and **automation** to enhance manufacturing efficiency by transforming digital designs into material products through an automated process, in opposition to traditional, time-consuming manufacturing methods. Another significant advantage is its ability to produce **customized** and **complex items** without the necessity for specialized tooling showing an incredible **flexibility**.
The rapid prototyping capabilities of 3D printing drastically cut down the time required to develop and test new products too. This increases the **speed** and **efficiency** of bringing products to market, giving companies a competitive edge.

Furthermore, additive manufacturing supports sustainable production practices by **minimizing material waste** and promoting localized production (49).

For all these reasons, there is no engineering field where AM techniques are not employes: from aerospace to biomedicine.

In the case of the **aerospace industry**, 3D printing has allowed the possibility of manufacturing large objects with complex dimensions drastically reducing the manufacturing time and costs, besides weight. The attainment of lightweight and complex-shaped samples in a short amount of time would have been challenging or even impossible to obtain employing traditional techniques.

However, additive manufacturing is a powerful technology because of its adaptability to a **broad dimensional range of products** too: from nanometric structures, normally

employed in bioengineering, to tens of meters, for the building construction.
Even if the construction process of **buildings** can be thought of as an additive manufacturing method from ancient times because of the sequential stacking of bricks, new devices for the continuous extrusion of concrete have been gaining traction in recent years (64). This has given space for creativity, resulting in the construction with ease and rapidity of buildings with particular geometries.

Within the field of **bioengineering**, instead, 3D printing has paved the way for new personalized healthcare implants, such as prostheses, medical devices or artificial organs (65). Focusing on bio-nanotechnologies, additive manufacturing is most employed in **tissue engineering** to produce three-dimensional scaffolds. These represent one of the key elements, besides cells and physical-chemical stimuli, in the generation of new artificial tissues. Scaffolds are supposed to mime the native extra-cellular matrix of tissues, in terms of composition and structure, in order to be colonized by cells. 3D printing is, thus, a valuable tool to create high resolution micro- and nanostructures with complex geometries. Contrary to traditional techniques, 3D printing produces more durable objects with controlled mechanical properties, such as isotropy or with mechanical strength gradients (66).

2.3.1 DLP printing of hydrogels

Among all the forementioned AM techniques, DLP is one of the finest manufacturing processes to print hydrogels, giving the possibility of creating gels with elaborate architectures.

Printing objects with high water content (more than 80%) can be challenging for several reasons. Firstly, there are not many water-soluble photo-initiators, and they are not very efficient compared to those soluble in organic solvents. Secondly, they nearly always require the employment of photo-absorbers to improve printing resolution, albeit this may not be optimal for biomedical purposes because dyes can be cytotoxic or can induce DNA damage (67).

Nevertheless, some examples of successful, biomedical or not, applications are available in scientific literature.
For instance, for the cardiovascular sector Ge *et al.* developed a multi-material **shape memory polymeric stent** in which the structural component was covered by a hydrogel. Hydrogel's main functionality was the slow release of drugs; tests conducted on an

artificial blood vessel showed that the release rate of loaded drugs was up to 90% within three hours (56,68).

Alternatively, Yang *et al.* fabricated a complex multi-material hydrogel that mimicked the structure and functions of a **heart valve**. CAD was retrieved through a reverse engineering process from computed tomography data, while mechanical tests showed excellent fatigue resistance of the hydrogel during cyclic experiments (56,69). This experience is noteworthy because it can pave the way for the substitution of small organs with artificial biocompatible ones in the optic of a more personalized medicine.

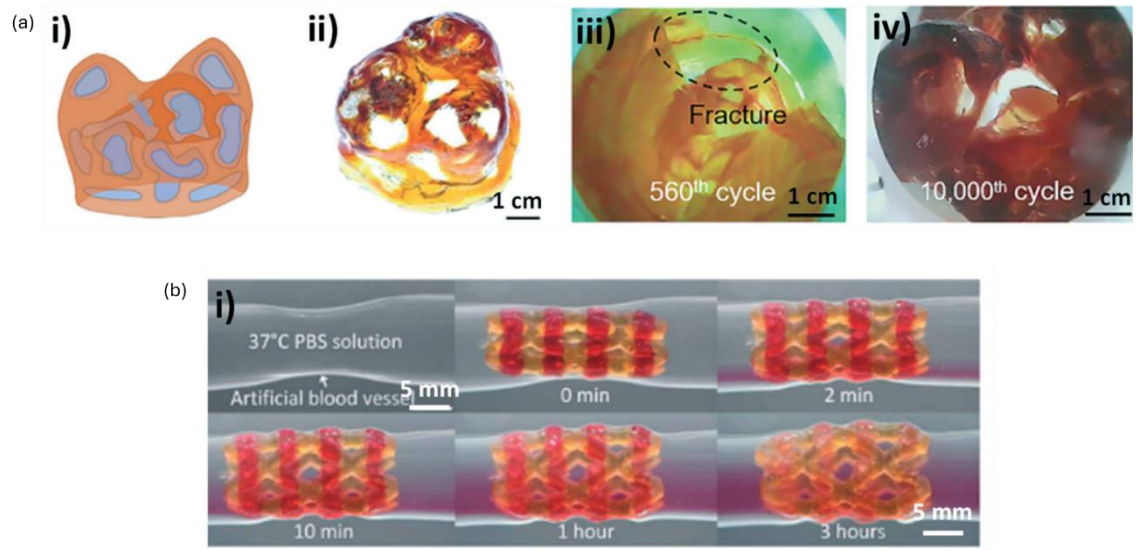

Figure 21 (a) DLP-printed structure mimicking a heart valve; (b) DLP-printed polymeric stent with drug release function.

DLP printing is a good strategy to also print **soft robots** and **soft electronics** for the same aforementioned reasons.

For example, an octopus-like **gripper** with eight arms has been fabricated by Zhongying *et al.*. This was able to selectively grip and release small objects if triggered by temperature (70), with a molecular mechanism similar to the one exposed in paragraph 1.2.

Zhang *et al.*, instead, produced an **electrical circuit** out of elastic materials, exploiting the hydrogel ability to conduct ions. They proved that the soft circuit maintained electrical functionality even under a large deformation (56,70).

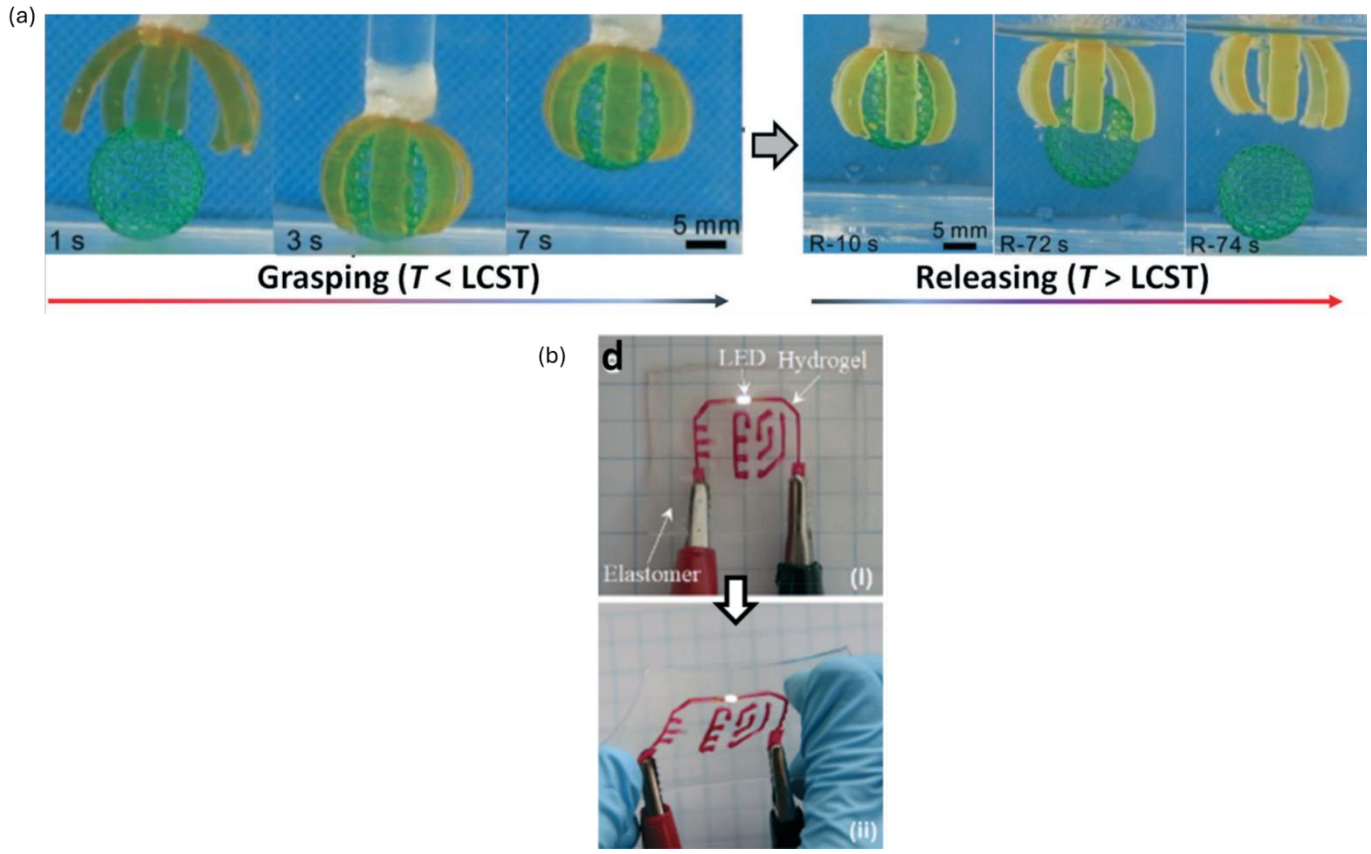

Figure 22 (a) DLP-printed gripper with thermal sensitivity, (b) DLP-printed soft electrical circuit.

3 MATERIALS AND METHODS

The aim of this work was to design a hybrid DNA-based hydrogel with acrylated PEG-derived backbone and to trigger it through the hybridization chain reaction process. A DLP 3D-printer has been employed to photopolymerize samples because of its several advantages, including the possibility of creating high-resolution objects at the micrometric scale. Then, hydrogels have been swelled in a solution containing complementary DNA-based fuel and their expansion has been evaluated.

3.1 MATERIALS

The **resins' formulation** was firstly inspired by Shi *et al.*'s work (45) in terms of materials' choice and relative concentrations, even though some modifications have been taken into account due to the disparity of available materials in laboratory and chosen methods. The main difference was the light source in the hydrogel fabrication process. In Shi's experience, a photolithographic process was performed into a homemade photolithography chamber at 365 nm UV light; while, in this thesis' work, a DLP printer with 385 nm UV light source was adopted because of the already cited several advantages. The pre-polymers' choice fell on polyethylene glycol diacrylate (**PEGDA**) 700 MW and polyethylene glycol methyl ether methacrylate (**PEGMEMA**) 950 MW. Both are biocompatible synthetic polymers used in a multitude of biomedical applications (71,72) when good mechanical properties are expected. Thanks to their acrylic endings that undergo a radical reaction in the presence of a UV-light activated photo-initiator, they are good candidates for the 3D printing process. As photo-initiators, lithium phenyl-2,4,6 trimethylbenzoylphosphinate (**LAP**) and water-soluble TPO based nanoparticle (**TPO-SDS**) have been compared. Two partially **complementary acrydite DNA strands** (described later) have been then added. Magnesium chloride has been dissolved in tris acetate-EDTA buffer (TAE) to obtain the final solvent (TAE/Mg^{2+}).

Some different DNA hairpins have been used to drive the hydrogel expansion and put in TAE/Mg^{2+} to create an **expansion buffer solution**. In analogy, non-complementary DNA strands have been used in a **control expansion buffer**. Those are reported in paragraph 3.1.2.

DNA was purchased by Integrated DNA Technologies, while all the others by Merck, except TAE/Mg^{2+}, that has been prepared in lab.

3.1.1 Solvent preparation

The role of the solvent is to protect and maintain all DNA strands in stable conditions. Thus, there was no reason not to take in consideration the same one used in Shi's experiment: TAE/Mg^{2+} which directs swelling within polymerization motor gels (45). **TAE solution**, in fact, has always been used with DNA strands, for example during gel electrophoresis, because it prevents from pH variations and enzymatic degradation, besides allowing the current to travel through the gel in gel electrophoresis (73). In addition, **Mg^{2+} ions** have been proved to mildly stabilize DNA hybridized structure thanks to the charge interactions with the phosphate backbone (45). As further precaution to avoid enzymatic degradation, nuclease-free distilled water (**H_2O^{N-}**) was substituted to the normal deionized one.

The protocol to produce TAE/Mg^{2+} buffer is the following:

1. Preparation of TAE 50x:
    a. Dissolution of EDTA in H_2O^{N-} and pH adjustment till pH 8.
    b. Dissolution of tris-base in H_2O^{N-} and slow addition of glacial acid and 0,5 M EDTA solution (pH 8).
2. Dilution of TAE 50x to 2x.
3. Dissolution of $MgCl_2$ in H_2O^{N-} in order to obtain a concentration of 25 mM.
4. Blend the same amount of TAE 2x and 25 mM $MgCl_2$. In this way the final concentration of TAE 1x and 12,5 mM of Mg^{2+} are obtained.

3.1.2 DNA strands

The choice of **eight specific oligonucleotides** was inspired by Cangialosi *et al.*'s experience (41): two of them are intended to join the hydrogel structure, four for the expansion buffer and the last two as control buffer (see Table 1). The ones put in the DNA-driven expansion buffer promoted the hybridization chain reaction. H1 and H2 were responsible for carrying on the expansion, while the terminator hairpins $H1_T$ and $H2_T$ controlled its termination. The control buffer was used only to demonstrate the specificity of the reaction, in fact the two DNA strands were not complementary to the ones in the hydrogel. They were purchased in a lyophilized form; however, to create the **mother solutions**, they were resuspended in TAE/Mg2+ with a concentration of 2 mM for all, except for the hydrogel ones whose concentration was 25 mM.

Hydrogel	
C	5’-/5Acyd/CTG TCT GCC TAC CAC TCC GTT GCG-3’
C’	5’-/5Acryd/ATT CGC AAC GGA GTG GTA GGC TTT-3’
DNA-driven expansion buffer	
H1	5’-AAA GCC TAC CAC TCC GTT GCG GAA CCT CGC AAC GGA GTG GTA GGC AGA CAG-3’
H2	5’-AGG TCC CGC AAC GGA GTG GTA GGC CTG TCT GCC TAC CAC TCC GTT GCG AAT-3’
$H1_T$	5’-AAA GCC TAC CAC TCC GTT GCG TCA AGC CGC AAC GGA GTG GTA GGC AGA CAG-3’
$H2_T$	5’-AGG TCC CGC AAC GGA GTG GTA GGC AAT CGT GCC TAC CAC TCC GTT GCG AAT-3’
DNA-driven expansion control buffer	
$H1_C$	5’-CCA GCG TGT GGC ACC TGC ACG CAC CCA CGT GCA GGT GCC ACA GCG AAC TTA-3’
$H2_C$	5’-TGG GTG CGT GCA GGT GCC ACA GCG TAA GTT CGC TGT GGC ACC TGC ACG TTG-3’

Table 1 List of oligonucleotides and their base sequences.

3.1.2.1 Hybridization process

The **hydrogel two** showed an **acrydite group** on the 5’ extremity so that they could photopolymerize together with the polymeric backbone. In order to expose only these terminations during the crosslinking reaction, C and C’ are supposed to hybridize. Thus, firstly they were diluted in the same 3 mM solution to perform a **thermal cycle** with Bio-Rad C1000 Touch PCR Gradient Thermal Cycler. It has been widely studied that temperature has an effect of DNA flexibility and its structure. Indeed, rising the temperature over a critic threshold (the melting point) allows the DNA to be more flexible (74,75) and to distend any potential random coil organizations. Furthermore, high temperatures can separate the two strands of a double-stranded DNA (dsDNA), whereas the slow decrease can re-pair them.

For this reason, temperature was set at 90°C and then, slowly lowered to 20°C in the most quasi-static way the machine could assure, namely the velocity rate was – 0,1 °C/s and for each variation of 10°C the cycle remained constant for 30 seconds, as in Figure 23.

For the same benefits, actually, also the **buffer hairpins** and the **control ones** received individually a similar heat treatment.

Figure 23 Thermal cycle to hybridize C and C' strands.

3.1.2.2 Verification of the hybridization process

At this point, an **electrophoretic run** was performed to verify if the DNA hybridization has occurred. It is a standard technique to separate DNA fragments according to their size and weight exploiting the fact that DNA is negatively charged.

The method involves an electrophoretic chamber, a buffer solution, a power source and an agarose gel indented at one extremity. Figure 24 (76) shows the **set-up**: the gel and the ion buffer solution are set into the chamber, then DNA samples are placed into the gel's indentations called wells and the power source is attached to the two extremities of the chamber.

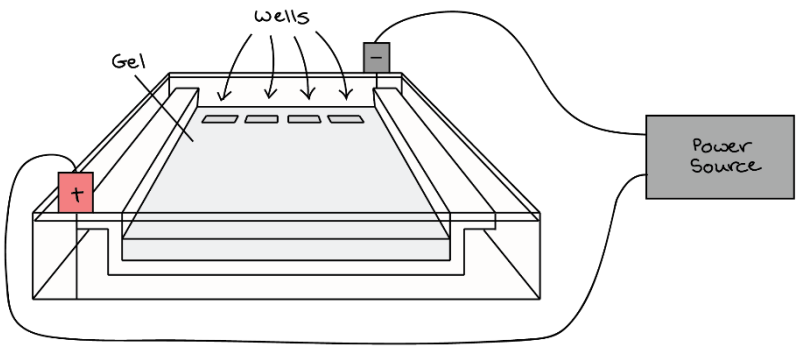

Figure 24 Set-up for the electrophoretic run.

Since DNA has a negative charge, it is attracted to the positive pole in the presence of an electric current, so it moves toward the opposite pole. Lighter fragments are less hampered by the gel's filaments, so they run faster, vice versa heavier fragments are slower. This results in a separation. In analogy single stranded DNA (ssDNA) are faster than double-stranded ones of the same length.

The **protocol** to create 1% w/v agarose gel is the following:

1. Weight agarose and place it in a glass bottle. It must be the 1% of TAE.
2. Add TAE 1x.
3. Place the bottle in a microwave for 30 seconds at the highest power to help the dissolution of the agarose. Occasionally, shake the bottle to help the process.
4. Once the solution is completely clear and a bit colder, add 10 μM in 100 mL gel of SYBR Safe 10.000x and shake.
5. Transfer the gel solution in a suitable mold to jellify at room temperature and create wells.
6. When the gel is ready, carefully remove the mold.

3.1.3 Resins' preparation

Since very few DNA is needed to show the expansion preliminary testing was performed with resins without it. When optimal formulation and parameters were determined, the DNA was added. As reported in Shi *et al.* (45), it was decided to maintain 10% wt of monomeric units, with or without the presence of 1,154 mM of double-stranded DNA (C-C'), in agreement with what mentioned above.

3.1.3.1 Photo-initiator choice

Since the light source for the photopolymerization was different from Shi's one in terms of wavelength, it was necessary to modify the photo-initiator used. Shi *et al.* used 2-hydroxy-1-[4-(2-hydroxyethoxy) phenyl]-2-methyl-1-propanone also called **Irgacure 2959** or I2959 which has the highest rate of absorbance at 276 nm, largely outside the range of the 3D printer emission spectrum. Some specifications are required when looking for a substitute: the ideal photo-initiator should absorb at higher wavelength (**385 nm**), be **water soluble** and have **low cytotoxicity**. Considering the limited variety of available photo-initiators with those characteristics, phosphine derivatives, such as **LAP** and **TPO nanoparticles**, seem to be the most suitable ones (77). Not only the type but also the amount of photo-initiator in the solution is an important factor as well because too little would lead to the formation

of few radicals and therefore non-polymerization, while too much would cause toxicity issues, especially in *in vivo* applications, where the radicals could interact with the surrounding biological environment (63).

A first evaluation on light absorbance and rheological properties was conducted on **three formulations** based on TAE/Mg^{2+} and 10% wt PEGDA, with the addition of:

- LAP 2% w/w
- TPO-SDS 5% w/w
- TPO-SDS 10% w/w

The proportion of the photo-initiator must be considered on the weight of the monomeric unit. In the case of TPO-SDS, it was added a higher content since in this case only part of the powder (around 10%) is of TPO photo-initiator, while the remaining 90% is constituted by a surfactant (SDS), which is not active in the photopolymerization process.

3.1.3.2 Addition of monofunctional pre-polymer

As showed later, LAP resulted to be a better photo-initiator, so it was always used in all the subsequent formulations.
Afterwards, DNA was added to the resin and expansion was performed. The **first formulation** prepared is here resumed:

- Monomeric unit: PEGDA 10% wt
- Photo-initiator: LAP 2% w/w
- Hybridized DNA: C-C’ 1,154 mM
- Solvent: TAE/Mg^{2+}

However, in a second set of experiments, monofunctional monomer **PEGMEMA** was inserted in the solution too to decrease the cross-linking density of the 3D network. Keeping constant the total of monomeric units as 10% wt of the final solution, different quantities of the monofunctional polymer were tested. More precisely, starting from the 1:1 formulation, the molar ratio between the polymers was varied by increasing the amount of one relative to the other and vice versa, as follows:

Formulation name	Molar ratio of PEGDA	Molar ratio of PEGMEMA
F11	1	1
F12	1	2
F13	1	3
F21	2	1
F31	3	1

Table 2 List of the formulations with different ratios of the components.

Resin called F21 seemed to be the optimal one for 3D printing, so the **final formulation** is here resumed:

- Monomeric units: PEGDA-PEGMEMA (2:1) 10% wt
- Photo-initiator: LAP 2% w/w
- Hybridized DNA: C-C' 1,154 mM
- Solvent: TAE/Mg^{2+}

The resins' preparation followed this **protocol**:

1. Preparation of a 10x LAP solution: dissolve LAP in TAE/Mg^{2+}.
2. Put the right amount of every ingredient in a 1,5 mL Eppendorf tube.
3. Stir with a vortex till the solution appears clear.

To avoid damages to DNA, solutions containing it were stocked at -20°C and thawed when needed, while the other ones, used as control, were normally stocked at room temperature.

3.2 UV/VISIBLE SPECTROSCOPY

To ensure that the absorption spectrum of the photo-initiator matches at least partially with the emission spectrum of the 3D printer's light source, BioTek Synergy HTX Multi-Mode Microplate Reader was used to accomplish an **UV/visible spectroscopy**. This is a standard laboratory technique that investigates how light interacts with matter at UV and visible wavelengths. Substances, in fact, selectively absorb light wavelengths when crossed by an optical radiation.

The UV/visible spectroscope set-up is made up of a light source that irradiates the sample with a wide range of wavelengths and a detector that captures the non-absorbed light, as in Figure 25 (78).

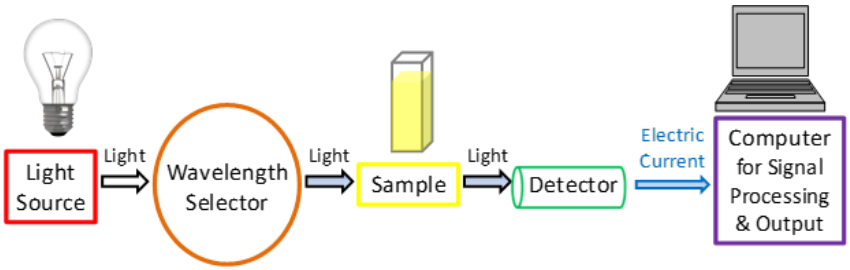

Figure 25 UV/Visible spectroscopy principle

The output signal is, therefore, processed showing the absorbance by varying the light wavelength. Absorbance is modelized by **the Lambert-Beer's law** (Equation 1) and depends on the molar extinction coefficient of the material (ε), its concentration (C) and the optical pathway of the radiation (z).

$$A = \varepsilon \cdot z \cdot C$$

Equation 1 Lambert-Beer's law

During this test, light was varied from 325 nm to 700 nm in 5 nm steps and the final photo-initiators' signal is obtained by subtracting contributes coming from TAE/Mg^{2+} and PEGDA.

3.3 RHEOLOGY

The rheometer Anton Paar MCR 302 with plate-plate configuration has been used to evaluate and compare the rheological properties of different formulations and their relative hydrogel samples.

Two different characterization methods can be performed:

- Steady shear characterization
- Oscillatory shear characterization

Steady shear characterization assesses the material's response to shear stress when the upper plate rotates continuously. The flow curve in which shear stress (τ) is related to shear rate ($\dot{\gamma}$) provides information about the solution's viscosity. Indeed, it is defined as follows:

$$\eta = \frac{\tau}{\dot{\gamma}}$$

Equation 2 Viscosity definition

Keeping constant the shear stress, if it doesn't change with the shear rate, fluids are called **Newtonian**, otherwise they have **shear-thinning** or **shear-thickening** behavior. Usually, polymeric solutions are shear-thinning, in other words their viscosity decreases as shear rate increases.

In this thesis work, **shear rate test** has been performed. It consists in fixing a range of shear rates and waiting for the rheometer's estimation for the relative shear stress, and viscosity consequently.

The set parameters were the following:

Parameter	Value
Plate-plate distance	200 μm
Shear rate	1 to 1000 1/s
Temperature	25 °C

Table 3 Shear rate test – Parameters

During the **oscillatory shear characterization**, instead, the upper plate rotates sinusoidally, and the viscoelastic properties of the material are evaluated. This kind of test provides information about the storage modulus G', which describes the elastic response to the deformation, and the loss modulus G'', which describes the viscous response.

The deformation's amplitude or frequency could be varied; **amplitude sweep tests** generally aim at describing the deformation behavior of the material, while **frequency sweep tests** its time-dependent behavior.

For this thesis work, only the amplitude sweep test on the solid hydrogel was interesting to assess. Figure 26 (79) shows a typical output graph of this test. The first region, in which G' and G'' are steady, is called linear viscoelastic region (LVE) and states the region in which the sample's structure is maintained and it is not destroyed. Exceeded the linear limit γ_L, micro-cracks occur in zone 1 but sample still maintains its structure till point 2, in which sample is eventually destroyed.

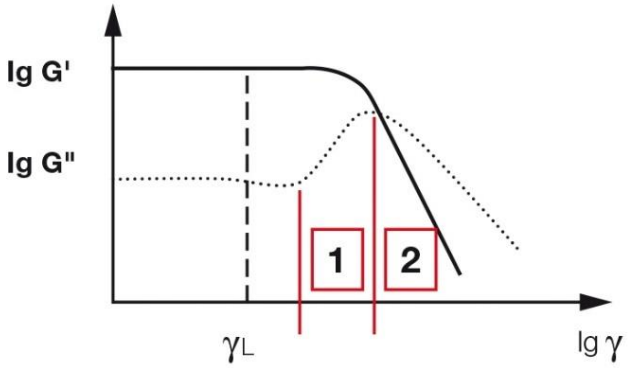

Figure 26 Output graph from amplitude sweep test

The set parameters for the test were the following:

Parameter	Value
Plate-plate distance	200 µm
Amplitude sweep	0,01 to 1000 %
Frequency	1 Hz
Temperature	25 °C

Table 4 Amplitude sweep test – Parameters

3.4 PHOTO-RHEOLOGY

In order to choose the most suitable resin for 3D printing and help finding the optimal printing parameters, photo-rheological tests were implemented too. Photo-rheology is, indeed, a technique to evaluate the **photo-polymerization kinetics** by measuring the rheological properties in the presence of UV or visible light. The test is very similar to the oscillatory rheological one, except for a few details: the lower plate should be made in quartz, to allow the light to pass through it, a UV or visible light source is needed and both deformation's amplitude and frequency are kept constant. For this latter reason, this test is called **time sweep test** because it only depends on time.

The protocol followed during this work was:

1. Measure G' and G'' of the liquid resin for 30".
2. Irradiate the sample for 150" while still measuring G' and G''. Normally, the irradiation ends when the plateau is reached but PEGDA-based resins are rapid to polymerize, so a constant time period for all the formulations is chosen.
3. Measure G' and G'' of the solid hydrogel for additional 20".

The employed UV light source was the UV Hamamatsu LC8 wide-spectrum lamp, and the set parameters were the following:

Parameter	Value
Plate-plate distance	200 µm
Amplitude sweep	1 %
Frequency	1 Hz
Temperature	25 °C

Table 5 Time sweep test – Parameters

3.5 HYDROGEL SAMPLE PREPARATION

Resins were photopolymerized in the Asiga Max X27 3D printer (Figure 28) to obtain the final hydrogel with desired shape. This device has a bottom-up setup based on the DLP technology (Figure 27, (80)): a LED light source that can generate 385 nm UV light is placed at the bottom of the machine and irradiates a platform that slowly rises layer-by-layer where the sample is printed upside down. The printer resolution depends on the size of the single irradiated pixel, and it is fairly fine: 27 µm on x-y plane, 1 to 500 µm on z axis. This means that this tool is so powerful that it can print objects with dimensions from tens of centimeters to hundreds of micrometers.

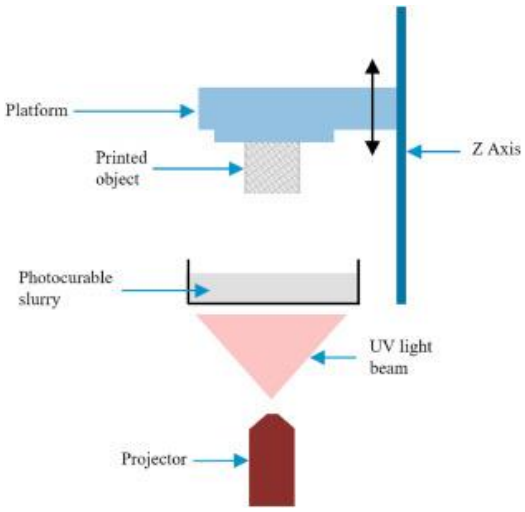

Figure 28 Schematic bottom-up approach of a DLP printer

Figure 28 Asiga Max X27

The 3D printing process is composed of four phases:

1. **CAD designing** with the help of a solid modeler software, such as SolidWorks, that was used during this thesis work.
2. **Printing parameters setting**.
   If a commercialized resin has been used, parameters are provided by the seller. Otherwise, if the formulation has been crafted in laboratory, it takes some time to optimize them. Commonly, the layer thickness, the light intensity and the UV exposure time are the most adjusted ones. Nevertheless, to further optimize the process in terms of process time and object resolution, some advanced ones could be modified as well if needed. In particular, the separation or approach velocity of the platform and the waiting times.
3. **Printing phase**:
   a. **Approach**: the platform approaches the vat on the top of which the resin has been placed.
   b. **Layer irradiation**: one layer at a time is photopolymerized.
   c. **Detachment**: the platform detaches from the vat to adjust the height and repeat the printing phase till the completion of all layers.
4. **Post-curing phase**: the printed sample is washed to remove the exceeding liquid resin trapped in it and to strengthen its properties.
   Actually, it was not deemed appropriate to stress the hydrogel with this additional step, to avoid any further DNA damage.

3.6 DNA-DRIVEN EXPANSION

3.6.1 Hydrogel swelling behavior

Hydrogel swelling properties are related to their high thermodynamic affinity for water-based solvents (81) and, when they are immersed in it, they tend to trap and retain it. The **swelling kinetics** is highly influenced by the composition of the polymeric network and by the type of solvent in which hydrogels are immersed. For this reason, it must be evaluated along the course of time.

During the swelling process, hydrogels could manifest two different behavior: a gravimetric or a volumetric expansion.

Gravimetric swelling is defined as the increment in hydrogel weight, due to the accumulation of solvent and it is estimated by measuring the hydrogel weight at different time point. Then the gravimetric swelling ratio can be analyzed as follows:

$$\text{Gravimetric Swelling Ratio} = \frac{W_s - W_i}{W_i}$$

Equation 3 Gravimetric swelling ratio (W_s = weight of the swollen hydrogel at each time point, W_i = weight of the hydrogel immediately after the crosslinking)

Alternatively, **volumetric swelling** is defined as the increment in hydrogel volume, due to the distension of polymeric chains because of the penetration of solvent molecules. Likewise, its swelling ratio can be measured as follows:

$$\text{Volumetric Swelling Ratio} = \frac{V_s - V_i}{V_i}$$

Equation 4 Gravimetric swelling ratio (V_s = volume of the swollen hydrogel at each time point, V_i = volume of the hydrogel immediately after the crosslinking)

3.6.2 Expansion protocol

As soon as hydrogel samples are printed, they are ready to the expansion process. However, since hydrogel are naturally able to swell, it is important to avoid the co-existence of the two phenomena and the protocol should be divided into two parts:

1. **Swelling** in TAE/Mg^{2+} so that the hydrogel reaches **saturation**. PEGDA-based samples swelled for 24 hours, in accordance with scientific literature (81,82), while PEGDA-PEGMEMA ones were leaved for 48 hours.
2. **Swelling** in a **proper expansion buffer** which contains complementary hairpins to start the hybridization chain reaction. This step was completed in 96 hours after the first one.

The expansion buffer contained only TAE/Mg^{2+} and 40 mM of each type of hairpins, with 98% of polymerizing ones (H1 and H2) and the remaining 2% of terminators ($H1_T$ and $H2_T$).

The analogous control buffer to verify specificity contained 40 mM of control hairpins. To correctly compare results, control experience followed the same procedure as the normal one.

In a first moment, printed hydrogels were placed into a multi-well plate to be swollen, however multiple difficulties have occurred between the first phase and the second one leading to the breaking of samples most of the times.
To minimize this risk, an **alternative set-up** has been arranged as in Figure 29. A PAP-Pen for immunostaining has been used to trace hydrophobic edges to separate samples onto a slide.
For each slot, 25 µL of the two swelling solutions have been poured and taken with a micropipette.
Then, the entire assembly has been collocated into a petri dish, closed by parafilm, to create a controlled environment to avoid the solvent evaporation.

(a)

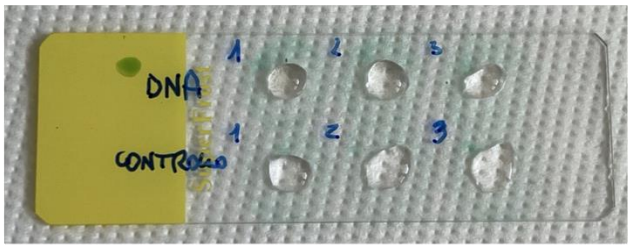

(b)

Figure 29 Swelling set-up: slide containing six slots for hydrogels (a) and controlled environment (b).

3.7 QUANTIFICATION OF DNA-DRIVEN EXPANSION

Even if the swelling test usually evaluates weight variations, the goal of this experience was to quantify the size expansion in geometrical terms. Thus, just after 3D printing and for each step of the previous protocol, samples were gently tapped onto absorbent paper and a **digital microscope** Andonstar ADSM301 (Figure 30) captured images of the top section of each one. The objective-sample distance was kept constant at 5,75 cm during all the measurements at the maximum magnification.

Figure 30 Digital microscope Andonstar ADSM301

Subsequently, Image Processing MATLAB tools helped counting the number of pixels corresponding to the area of the hydrogel. Specifically, a region of interest (ROI) was manually taken thanks to **Image Segmenter** and converted in a binary file (Figure 31).

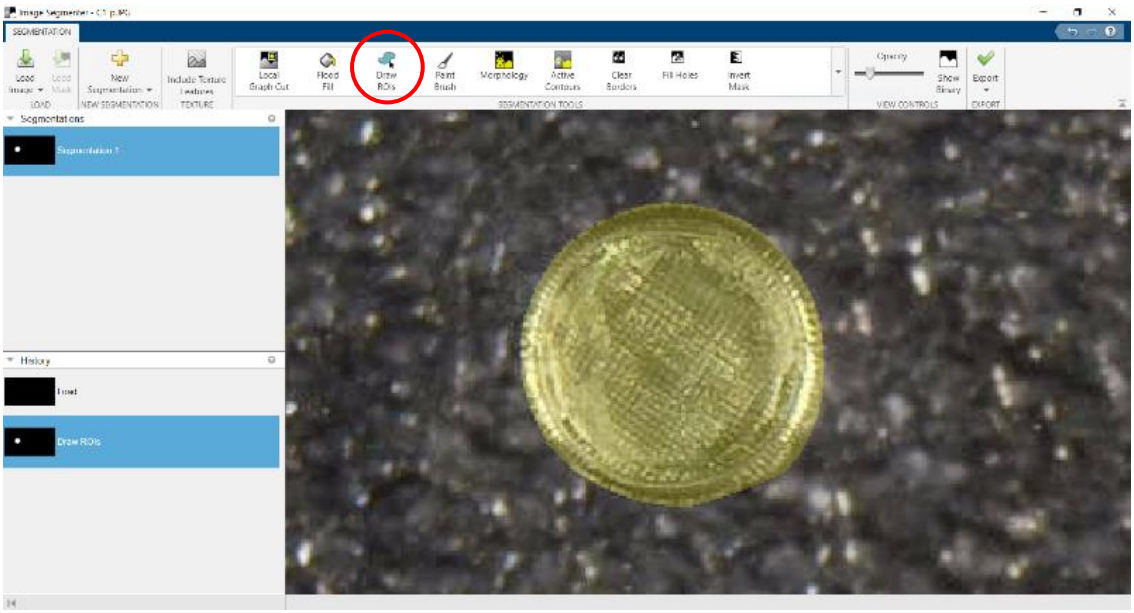

Figure 31 Image Segmenter by MATLAB

Then, **Image Region Analyzer** returned data about the ROI area as number of pixels (Figure 32).

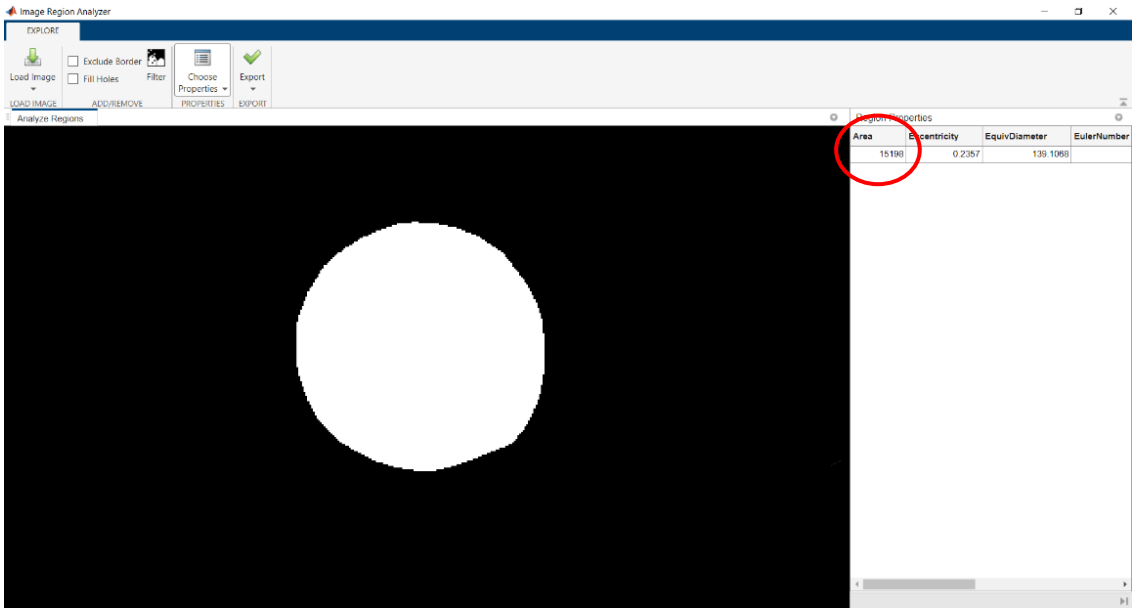

Figure 32 Image Region Analyzer by MATLAB

At this point, ImageJ was used to identify the correspondence between number of pixels and millimeters (1 mm = k px) and the conversion in mm^2 was easily made thanks to the following equation:

$$A_{mm^2} = \frac{1}{k^2} \cdot A_{px}$$

Equation 5 Area conversion from pixels to mm^2

Unfortunately, samples were too frangible to measure both surface area and height, so it has been decided to evaluate hydrogel swelling only through its surface variation.
The **surface swelling ratio** (**SSR**) has been defined as follows:

$$\text{Surface Swelling Ratio}_{\%} = \frac{S_s - S_i}{S_i} \cdot 100$$

Equation 6 Gravimetric swelling ratio (S_s = volume of the swollen hydrogel at each time point, S_i = volume of the hydrogel immediately after the crosslinking)

3.8 DATA ANALYSIS

Once data have been measured and a dataset has been made up, a statistical elaboration has been required. For each trial, six replicates of DNA-based sample and six of DNA-free ones have been evaluated, then their SSR values have been presented as **mean ± standard deviation**.

Since they were few samples, SSR values were complemented by statistical tests to assess the statistical significance of the outcomes.

The most appropriate test to determine whether samples grew over time was the **paired Student test** (paired t-test). This test evaluates if the mean difference between two sets of observations is null. In other words, if samples grew, they don't have the same mean, so the difference between the mean values is not null, otherwise it is zero.

Consequently, the competing hypotheses for the variable $\mu_d = \mu_{obs1} - \mu_{obs2}$ are:

$$\begin{cases} H_0: \mu_d = 0, & \text{null hypothesis } (\mu_{obs1} = \mu_{obs2}) \\ H_1: \mu_d \neq 0, & \text{alternative hypothesis } (\mu_{obs1} \neq \mu_{obs2}) \end{cases}$$

Equation 7 Hypotheses for the paired t-test.

As most of statistical tests, the paired t-test requires several assumptions to be verified (83):

- The variable μ_d should not contain any **outliers**. They were removed before the beginning of the statistical analysis to avoid a bias in results.
- Observations must be **independent** of one another. It can be reasonably assumed since the same samples were measured at two different time points.
- The variable μ_d must be **continuous**. Samples' surface area is a value belonging to real numbers, so the difference between two surface area is still a real value.
- The variable μ_d must follow a **normal law**.

Several tests are available to assess normality of data. In this thesis work the **Shapiro-Wilk's** one has been picked because in literature it has been considered as the most powerful test for small datasets (number of samples < 30) and kurtosis less than 3 (84).

The competing hypotheses for this latter test are:

$$\begin{cases} \mathrm{H}_0\text{: normal data,} & \text{null hypothesis} \\ \mathrm{H}_1\text{: not normal data,} & \text{alternative hypothesis} \end{cases}$$

Equation 8 Hypotheses for Shapiro-Wilk's test.

Considering a **confidence interval** of **95%**, the null hypothesis was rejected for p-values less than 0,05 for both tests.

Therefore, the followed protocol was:

1. Performance of the Shapiro-Wilks test, thanks to a MATLAB algorithm available one the internet (85).
2. Analysis of the kurtosis and results from the Shapiro-Wilks test.
3. If all data were normal, performance of the paired Student test, thanks to the MATLAB function ttest().
4. Analysis of results from the paired t-test.

4 EXPERIMENTAL RESULTS AND DISCUSSION

This chapter will report and discuss the results obtained during the experimental part of this thesis work. Mainly it will be divided into two sections that follow the chronological order of the experiences: the first one about PEGDA-based hydrogels and the second one about the PEGDA-PEGMEMA-based ones. Each section will develop the early characterization stage of hydrogels not containing DNA and, only subsequently, the complete experiment on final DNA-based hydrogels.

4.1 PEGDA-BASED HYDROGELS

4.1.1 Photo-initiator's choice

Since high intensity UV light could damage DNA sequences (86), it was decided to work at longer wavelengths in the UV spectrum and, to evaluate the most suitable photo-initiator for the experience, TPO-SDS and LAP have been compared.

4.1.1.1 Optical spectroscopic analysis

First of all, the **UV-visible spectroscopy** has been performed to meet the absorption requirement of 385 nm due to the 3D printer light source. Initially, the three formulations (described at page 39), the positive control (formulation containing the same amount of PEGDA and 5% w/w of Irgacure 2959) and the negative one (only TAE/Mg^{2+} and PEGDA) were prepared. Since absorbance is an intrinsic property of the material, it does not depend on its concentration, so only one TPO-SDS formulation was tested. In a second time, untreated absorbance spectra from the plate reader were collected and processed by subtracting the negative control data from the others. In this way, it was ensured that only the photo-initiators' spectra were shown, as in Figure 33.

As expected from scientific literature (63), at 385 nm TPO nanoparticles and LAP absorb a higher amount of UV light than Irgacure 2959 because this wavelength belongs to their activation range (320-390 nm). Thus, since both could be used and have similar properties in terms of water solubility and cytotoxicity, other methods were required to discriminate the best one.

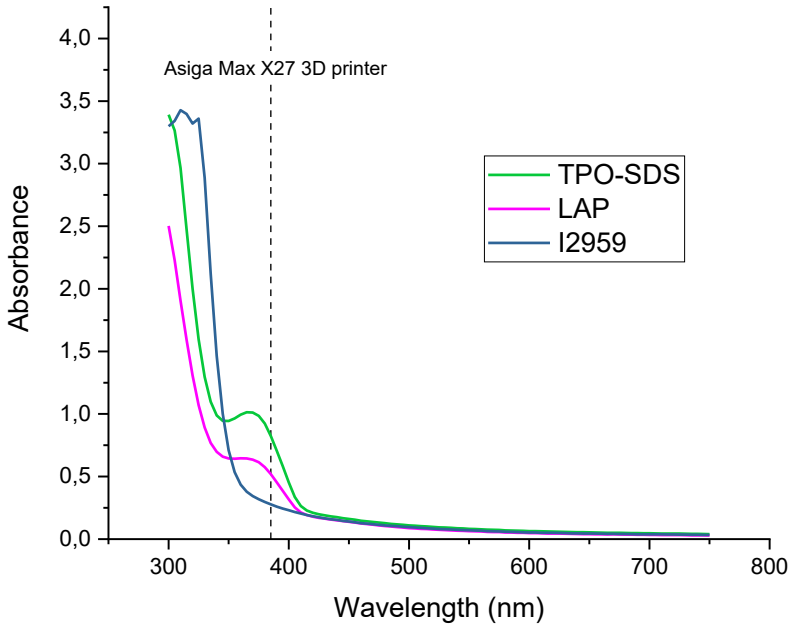

Figure 33 Absorbance spectra of three different photo-initiators and highlight of 3D printer wavelength (385 nm).

4.1.1.2 Rheological and photorheological analysis

Rheological and **photorheological tests** provide an indication of resins' printability, which is influenced by photo-initiators.

In DLP printers, the platform movement generates a shear rate (Equation 9, (87)) that influences the resin's viscosity.

$$\dot{\gamma} = \frac{\nu}{e}$$

Equation 9 Shear stress in DLP printers is function of the separation/approach velocity (ν) and layer thickness (e).

Typically, in order to assure a uniform redistribution of the formulation during the printing process, resins' viscosity must be lower than 5 Pa·s (88) and must have a shear-thinning behavior. Results of the **shear rate test** can be seen in Figure 34 and state that all the PEGDA-based formulations respect the printing requirements.

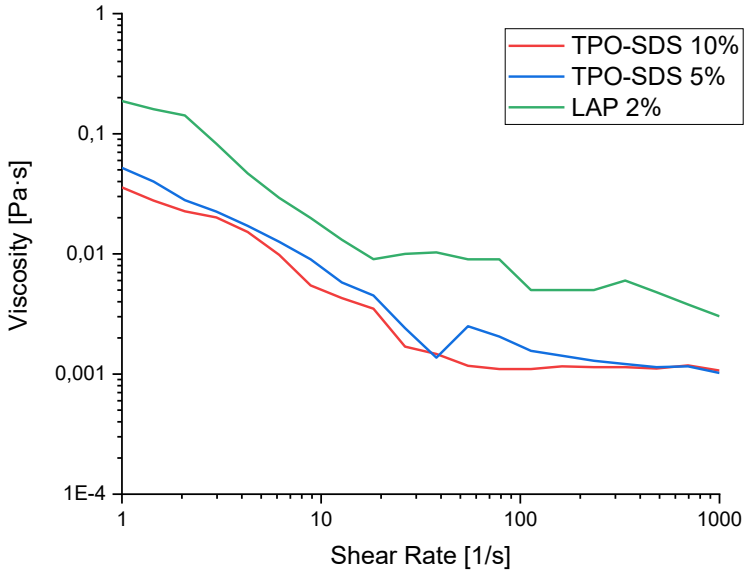

Figure 34 Viscosity, as function of shear rate, of PEGDA-based formulations with different photo-initiators.

The **amplitude sweep test** was needed to find the LVE region critical limit (γ_L) in order to set a constant strain during the photorheological test that is included in the LVE range. Results of this test are reported in Figure 35 and the critical value γ_L has been estimated as follows:

Formulation	Linearity limit γ_L
TPO-SDS 10%	6%
TPO-SDS 5%	10%
LAP 2%	20%

Table 6 Linearity limit γ_L for PEGDA-based formulations with different photo-initiators.

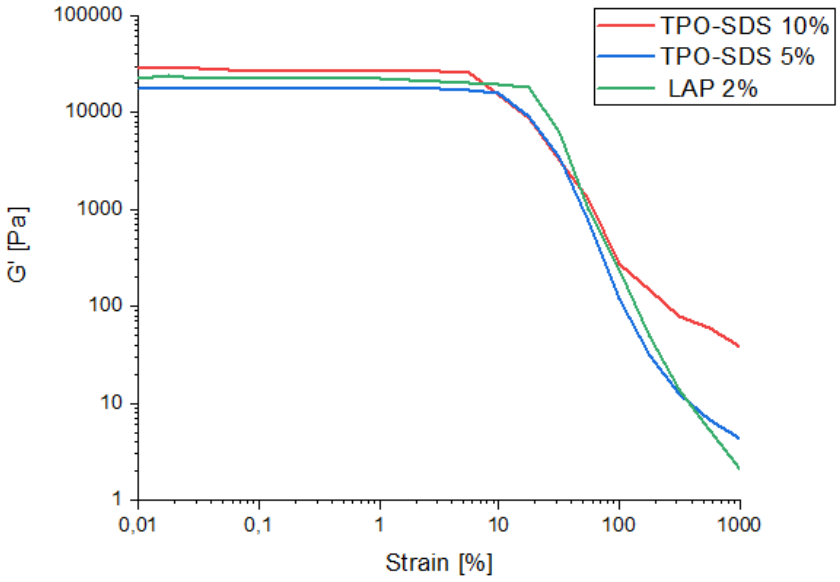

Figure 35 Amplitude sweep test of PEGDA-based formulations with different photo-initiators.

Considering these results, amplitude sweep for the **photorheological analysis** was set at 1% and the **time sweep test** was performed, obtaining the trends shown in Figure 36.

It can be observed that the photo-initiator choice still does not really affect the formulation's performance. All the resins rapidly photopolymerize and their storage moduli reach high comparable values, meaning that printing times are expected to be brief and hydrogels sufficiently resistant to stress. To delve deeper into details, the formulation containing LAP solidify just a bit faster than the two with TPO nanoparticles while the storage modulus of the final samples is impacted by the amount of photo-initiator. The hydrogel with the higher content of TPO-SDS is also the one which showed higher G' values, whereas the one with LAP has intermediate mechanical properties even if it has the lower proportion. This can be explained by remembering that the amount of TPO in TPO-SDS nanoparticles is only the 10% w/w, so that a higher quantity of the entire complex is needed to have comparable effects with LAP molecules.

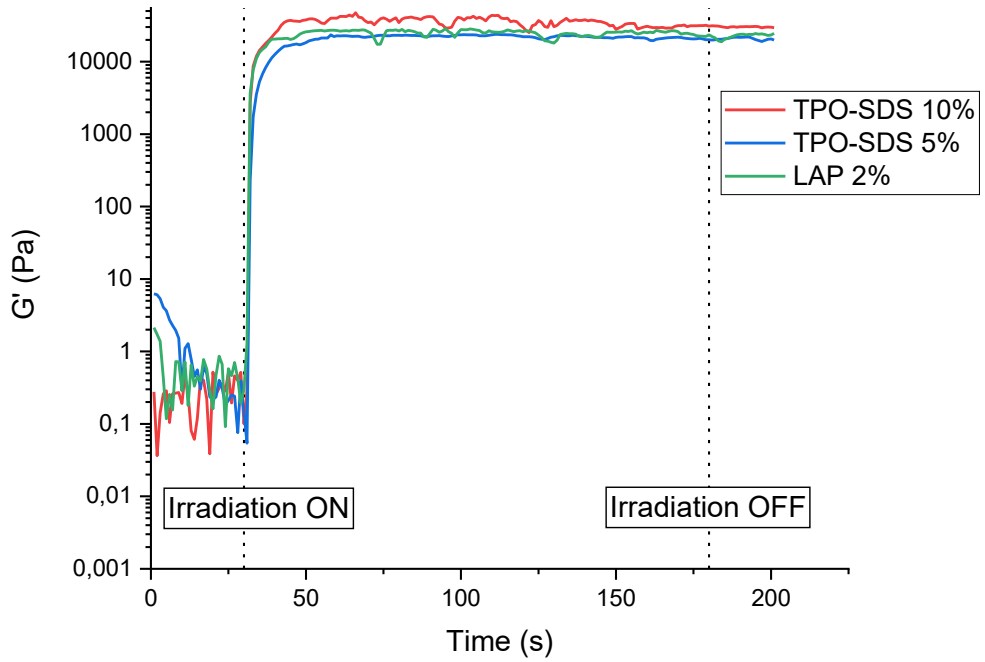

Figure 36 Time sweep test of PEGDA-based formulations with different photo-initiators

Overall, LAP seemed to be the most suitable photo-initiator because:

- It can photopolymerize almost instantaneously
- It is naturally water-soluble
- It produces reduced cytotoxic effects thanks to the insignificant quantity needed
- It allows the hydrogels to be more mechanically resistant, e.g. by tolerating higher strains before failing (see Figure 35).

Thus, it has been chosen for all the following steps and further formulations.

4.1.2 3D-printing

At this stage, attention was focused on the printability of the PEGDA-based formulation before the addition of DNA strands to the final resin. Samples' geometry was chosen, and printing parameters were researched.

4.1.2.1 Computer-Aided Design

Since the DNA hybridization-chain reaction is a microscopic process, particular care has been taken to samples' dimensions. Indeed, assuming the length of a nucleotide as 0,33 nm (89), it can be estimated that each DNA strand in the expansion buffer solution is approximately long 20 nm. Therefore, taking into account the fact that each strand partially overlaps and neglecting for a moment any other side effect that can reduce the dimensions of each DNA chain, a significative macroscopic effect cannot be expected, especially on big samples.
Bearing this in mind and still aiming to show a macroscopic effect, it was deemed that the most appropriate dimensions were on the order of, at most, one millimeter.

Regarding shapes, instead, the following three **simple geometries** and three **complex** ones have been conceived thanks to the help of SolidWorks:

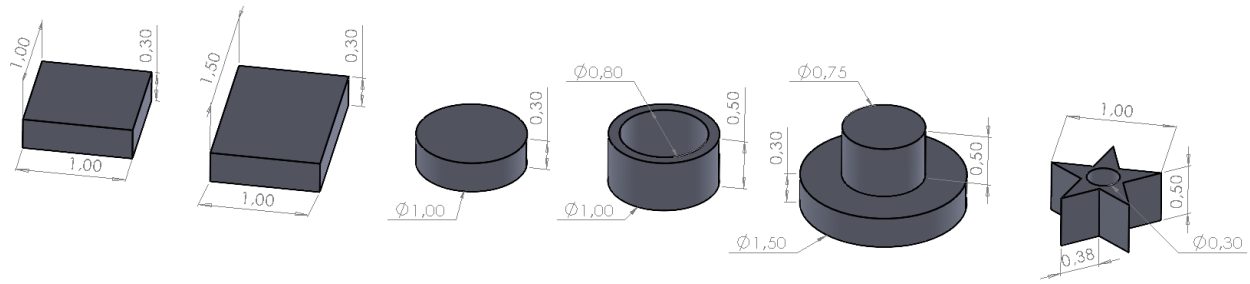

Figure 37 Employed CADs with quotes in millimeters. From the left side: square-based parallelepiped, rectangular-based parallelepiped, cylinder, holed cylinder, stacked cylinders, holed star-based prism.

While the simpler CADs served to verify the formulations' printability and to quantify the subsequent DNA-driven expansion, the more complex ones challenged the DLP printer capabilities and attempted to provide a visual idea of the expansion. In detail, the purpose of printing the holed cylinder and the star-based prism was to proof the printability, respectively, of 100 µm-thick walls and high-resolution details as the star arms. Each one of the two stacked cylinders, instead, was printed with a different material to test the multi-material printing.

4.1.2.2 Printing parameters

Initially, printing parameters were retrieved from scientific literature (90) and previous works on PEGDA-based formulations with similar pre-polymer molecular weight and concentration, albeit they needed to be adjusted to match with the specific formulation of this work. Besides good resolution, the minimal UV dose was sought with the aim of causing the least possible damage to the DNA when added. After several tries, the parameters in Table 7 have been chosen to print simple geometries.

	Burn-in	**Other layers**
Number of layers	8	till the end
Layer thickness [µm]	25	25
Exposure time [s]	2,5	2
Light intensity [mW/cm^2]	30	30
Separation velocity [mm/s]	2	2
Approach velocity [mm/s]	2	2

Table 7 Printing parameters of PEGDA-based resins - simple CADs

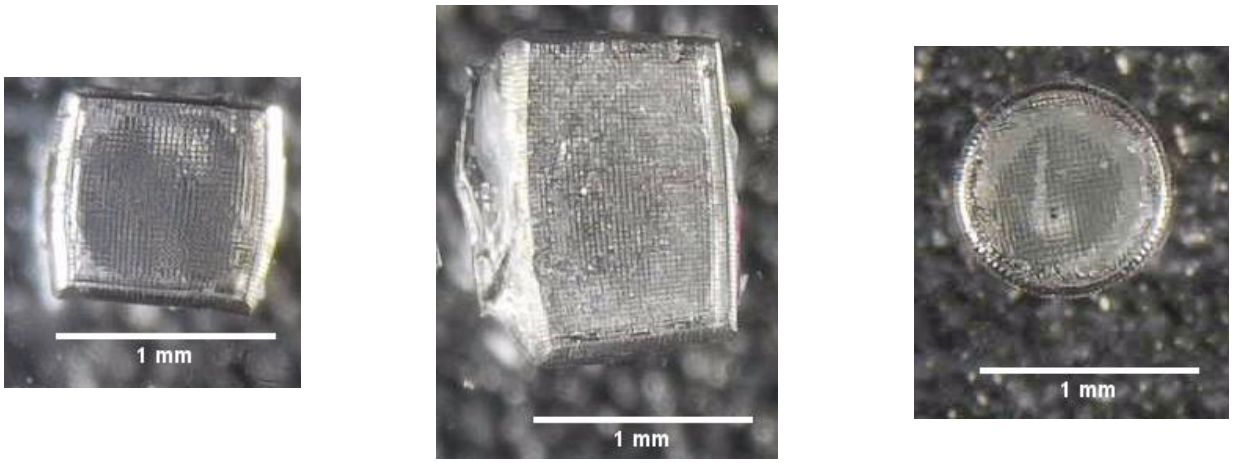

Figure 38 Top view of printed samples with simple geometries.

The original thickness of hydrogels was 1 mm on the z axis; however, it has been demonstrated that it could be lowered to 300 µm without the risk of breaking samples during the removal from the printing platform. Noteworthy, the printed structures clearly show XY pixel patterns on the surface, indicating outstanding printability.

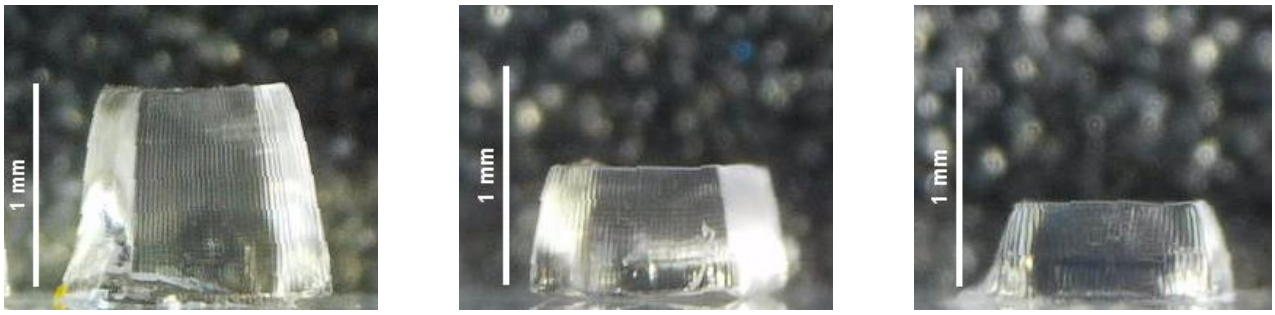

Figure 39 Side view of printed samples with square-based prism geometry. Height from left: 1 mm, 500 µm, 300 µm.

For complex geometries, instead, parameters had to be modified once again because the liquid resin kept on getting stuck in the holes, which consequently remained clogged. The new ones are resumed in Table 8.

	Burn-in	**Other layers**
Number of layers	3	till the end
Layer thickness [µm]	75	75
Exposure time [s]	1	1
Light intensity [mW/cm^2]	45	45
Separation velocity [mm/s]	1	1
Approach velocity [mm/s]	1	1
Wait time (after separation) [s]	2	2

Table 8 Printing parameters of PEGDA-based resins - complex CADs

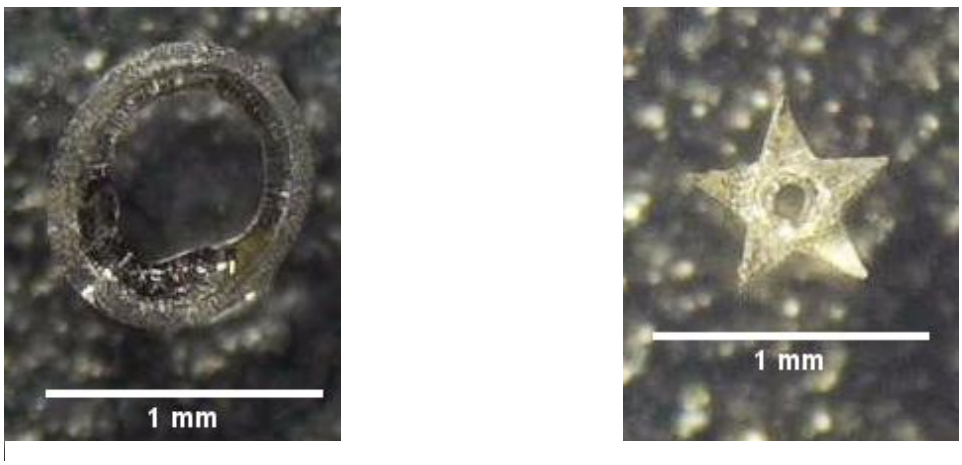

Figure 40 Top view of printed samples with complex geometries.

4.1.2.3 Overcoming printing difficulties

3D printing of hydrogels can be very challenging due to the high-water content that can give rise to several difficulties. Water-based resins, in fact, have a very low viscosity and are prone to deform or collapse under their weight during the printing process (56).
This latter problem can be normally solved by the addition of a photo-absorber to the photocurable resin, however in the case of this work it was not possible to proceed in this way due to the presence of DNA. From the scientific literature, it has been observed that certain dyes, e.g. tartrazine, have an ambiguous effect on DNA leading to DNA aberrations (67). Thus, it was decided to avoid any factor that could potentially spoil DNA and invalidate the DNA-driven expansion process.

Contrary to all expectations, the previous paragraph has shown that the former printing parameters have conducted to a **good structural integrity** and an **acceptable shape fidelity** of hydrogels even in the absence of the photo-absorber. This could already be considered an outstanding result; however, the printing process has been further optimized.
Thanks to the bottom-up configuration of the employed DLP printer, it has been possible to dispense **very few amounts of resin** managing to print, after several attempts, three samples in parallel with only 15 µL of resin.
Figure 41 depicts the difference between a standard quantity of resins for normal-dimensioned hydrogels (in the order of one centimeter) and the amount used at each printing during this experience. To better appreciate the difference, a blue dye has been added to the transparent resin.

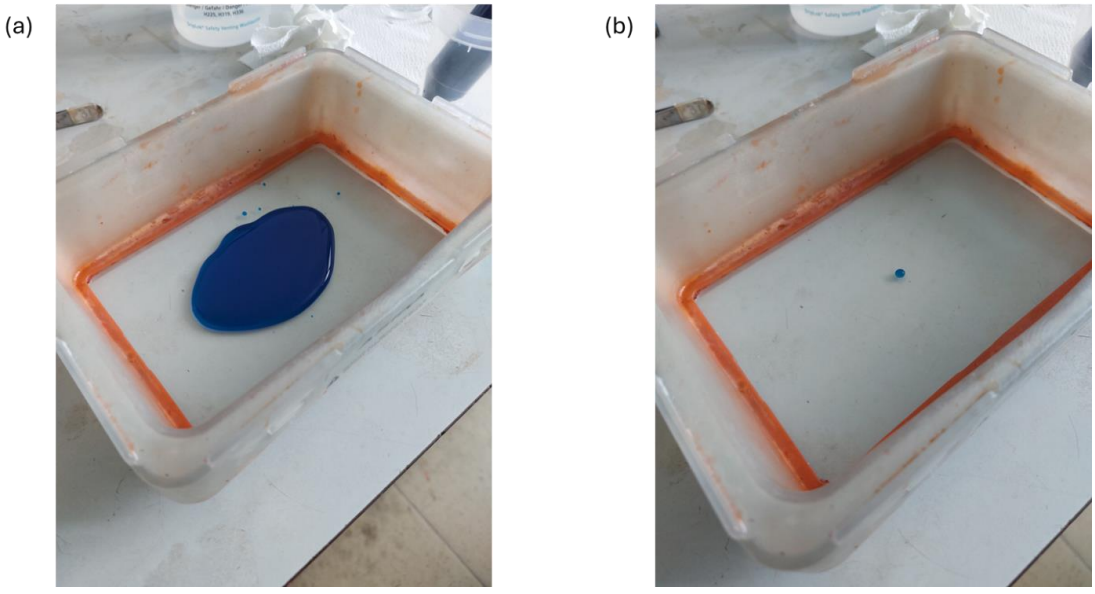

Figure 41 Standard amount of resin (a) vs amount of resin employed at each printing during this experience (b).

4.1.3 DNA formulation

The PEGDA-based formulation has shown, as expected, good printability so 1,154 mM of hybridized C-C’ dsDNA was added to the solution in order to print samples and submit them to the expansion protocol.

4.1.3.1 Verification of the hybridization

Before being included in the final solution, C and C’ ssDNA chains were dissolved in TAE/Mg^{2+} and subjected to a thermal cycle to get hybridized. To verify that this process successfully accomplished, electrophoresis on agarose gel was performed.

According to theoretical knowledge, a dsDNA complex runs slower on the agarose gel than a single strand of the same length because it is heavier and, if all the components of the same DNA solution are equally long, only one band should be macroscopically seen because they have the same run velocity.
Results reported in Figure 42 confirmed the hypothesis. C and C’ strands (respectively column c and b) have the same length but different content of base types, so their molecular weight is similar but not equal and they also are considerably faster than the control ladder, which is made up of dsDNA. Column d clearly showed the presence of a marked single bar in a higher position that the previous two, meaning that they properly hybridized.
With an in-depth look, it can be deduced that:

- C and C’ did not aggregate in weird complexes with different molecular weight because only one bar appeared.
- C and C’ strands coupled together in complexes with same base-pair length than the single strands because the d-bar is slightly higher than bars at column b and c.
- All the C and C’ molecules joined together since the bar color is significantly darker than the other two’s, suggesting that both strands are concentrated together.

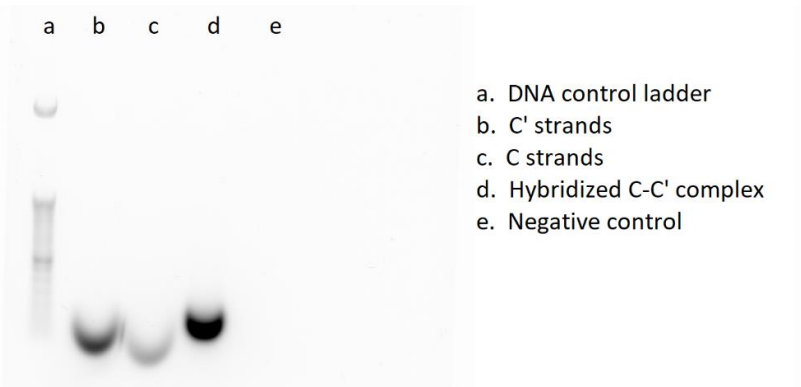

Figure 42 Top view of agarose gel after the electrophoretic run.

4.1.3.2 DNA-driven expansion

After conducting the required verifications, the desired formulation containing DNA and PEGDA was prepared. The DNA concentration was so low that did not consistently influence the rheological properties of the PEGDA-based resin; hence, the same aforementioned printing parameters were used to produce samples. Macroscopically, DNA-based hydrogels did not show any substantial differences from the ones leaking in it: both were well defined and transparent.

To guarantee statistical evidence, the DNA-driven expansion protocol was performed on six DNA-based samples (named “DNA” from now on) and six DNA-free ones (named “Control”).

The arrangement of the polymeric network in PEGDA-based hydrogels has an effect on both gravimetric and volumetric swelling when they are immersed in water (81). For this reason, to stabilize the volumetric swelling, printed samples were kept swelling in TAE/Mg^{2+} for 24 hours.

Since samples were hard to handle due to their frangibility and small dimensions, expansion was evaluated by comparing only the surface area variation, as in Figure 43. During the swelling in the first ionic solution, both DNA and control showed a similar behavior: DNA’s SSR was 20,37 ± 19,19 %, while control’s one 21,13 ± 12,67 %. Once hydrogels’ dimensions reached equilibrium, the first swelling solution was removed, samples were gently tapped onto absorbent paper and the new buffer solution containing complementary DNA hairpins was added and leaved for 96 hours. DNA’s surface further increased by 10,08 ± 9,34 %, whereas control slightly decreased by -0,30 ± 6,40 %.

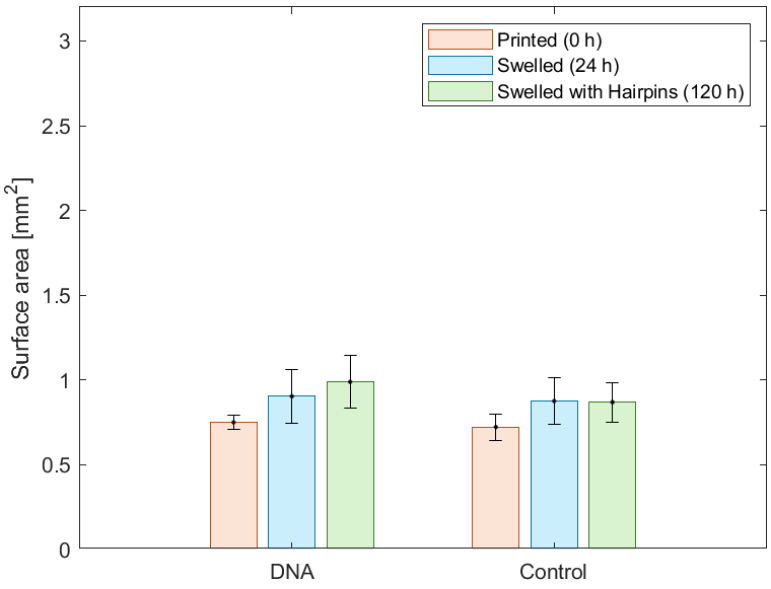

Figure 43 Surface area of PEGDA-based samples during the three steps of the DNA-driven expansion.

At a first look, the experience appeared successful: firstly, both DNA and control expanded with the same proportion; then, during the second phase, only DNA increased its dimensions thanks to the hybridization chain reaction, while control reached the swelling equilibrium and it was not affected by DNA hairpins.
Nevertheless, the standard deviation values suggested that the data are highly unlikely to be reliable, as they were comparable to the mean expansion values. Therefore, deeper statistical analyses were indispensable to support or contradict the hypothesis of DNA-driven expansion.

A **paired t-test** has been implemented at each step of the expansion protocol for both types of samples with particular interest on the second phase, that is the true DNA-driven expansion.
If the expansion were successful, the sample would, on average, have different dimensions at each stage, so values would have different means.
The variable x for this test is the difference between values at different times, namely:

$$x = \begin{cases} \text{swelled} - \text{printed}, & \text{during the } 1^{\text{st}} \text{ phase} \\ \text{swelled with hairpins} - \text{swelled}, & \text{during the } 2^{\text{nd}} \text{ phase} \end{cases}$$

Equation 10 Student test variables during the two phases of the expansion protocol.

Initially, the hypothesis of the variable normality was proven by the **Shapiro-Wilks test**, obtaining the following results:

		p-value	Kurtosis	Result
DNA	1st phase	0,16	1,66	Normal distribution
	2nd phase	0,36	2,03	Normal distribution
Control	1st phase	0,80	2,38	Normal distribution
	2nd phase	0,08	2,21	Normal distribution

Table 9 Shapiro-Wilks results for PEGDA-based samples.

Then, it was possible to proceed with the **paired Student test** that produced the following outcomes:

		p-value	Result
DNA	1st phase	0,08	Same mean
	2nd phase	0,08	**Same mean**
Control	1st phase	0,03	Different mean
	2nd phase	0,79	**Same mean**

Table 10 Student test for PEGDA-based samples.

It can be deduced that both types of samples had averagely the same dimensions before and after the swelling in the expansion buffer, demonstrating that the DNA-driven expansion **failed**.

Comparing this experience to Shi *et al.*'s one (45), despite the negligible differences in resin composition and fabrication method, a similar result can be found out. In fact, drawing attention to Shi's PEGDA 575 MW hydrogel in Figure 44 (45), it can be noticed that its expansion is close to 0% after the sixty-hour stay in the expansion buffer solution.

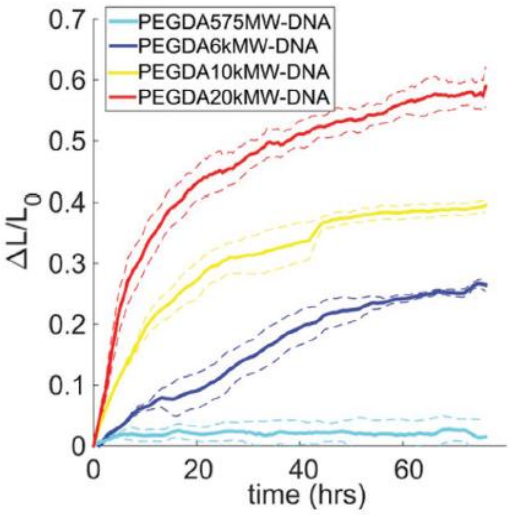

Figure 44 Shi *et al.*'s DNA-driven expansion results for PEGDA-based samples.

A possible explication can be argued by reflecting on the microscopical structure of the polymeric network. As a matter of fact, PEGDA 700 MW (and lower MW) is a relatively short pre-polymer which forms very **tight meshes** during the crosslinking. Consequently, even if DNA hairpins of the buffer solution reached the acrydite-DNA linked to the network, they were too constrained into strong meshes to evidently expand them through the cascading process.

Thus, **two potential solutions** can be implemented to broaden meshes:

- To use PEGDA with higher molecular weight, as Shi *et al.*'s did.
- To introduce monofunctional molecules in the resin formulation that can interfere with PEGDA.

4.2 PEGDA-PEGMEMA-BASED HYDROGELS

Since the first possibility has already been explored and high molecular weight PEGDA can come at high prices, the second pathway has been contemplated in this thesis work. No specific requirements were demanded to the monofunctional polymer except for the adequate chain length and an acrylic ending, hence PEGMEMA 950 MW has been selected among the PEG-derived molecules. The presence of this monofunctional monomer is intended to decrease the cross-linking density of the network, hopefully helping the DNA driven volume increase.

Furthermore, scientific literature leaks in studies on the impact of PEG-derived monofunctional polymers on PEGDA hydrogels. For this reason, further investigations on the resin composition were conducted before proceeding with DNA-driven expansion.

4.2.1 Choice of PEGDA-PEGMEMA proportion

Still keeping constant the total amount of monomers in the resin formulation, five different proportion of PEGDA-PEGMEMA (described earlier at the paragraph 3.1.3.2) have been compared in order to choose the most suitable one for the purposes of this experience, which are good printability and greater swelling.

Beamish *et al.*'s study (91), one of the few on this subject, showed that hydrogel's stiffness decreases and the swelling ratio increases with the increase of PEGMEMA within the formulation, in accordance with theoretical expectations. For this reason, formulations with more PEGMEMA than PEGDA were initially considered (F12, F13), and only then those with progressively lower amounts of PEGMEMA (F11, F21, F31).

4.2.1.1 Rheological and photorheological analysis

As for PEGDA-based formulations, printability was first evaluated by analyzing the rheological and photorheological properties of the formulations.

The **shear rate test** confirmed that all the formulations have adequate viscosity to be printed (lower than 5 Pa·s (88)):

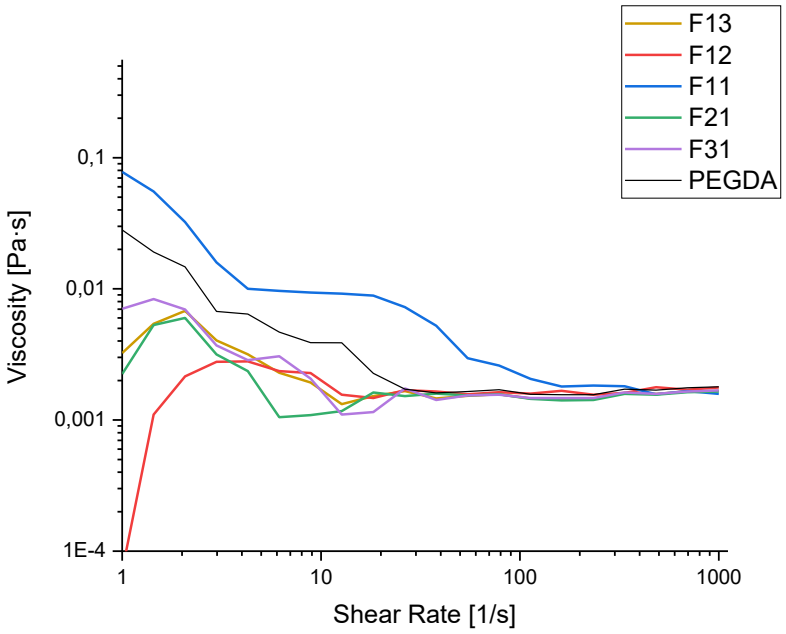

Figure 45 Viscosity, as function of shear rate, of PEGMEMA-based formulations.

Then, the **amplitude sweep test** has been performed on solid hydrogel to find the LVE region and estimate its critical limit (γ_L), obtaining the following values:

Formulation	Linearity limit γ_L	
F13	/	Not polymerized
F12	200%	
F11	100%	
F21	90%	
F31	60%	

Table 11 Linearity limit γ_L for PEGMEMA-based formulations.

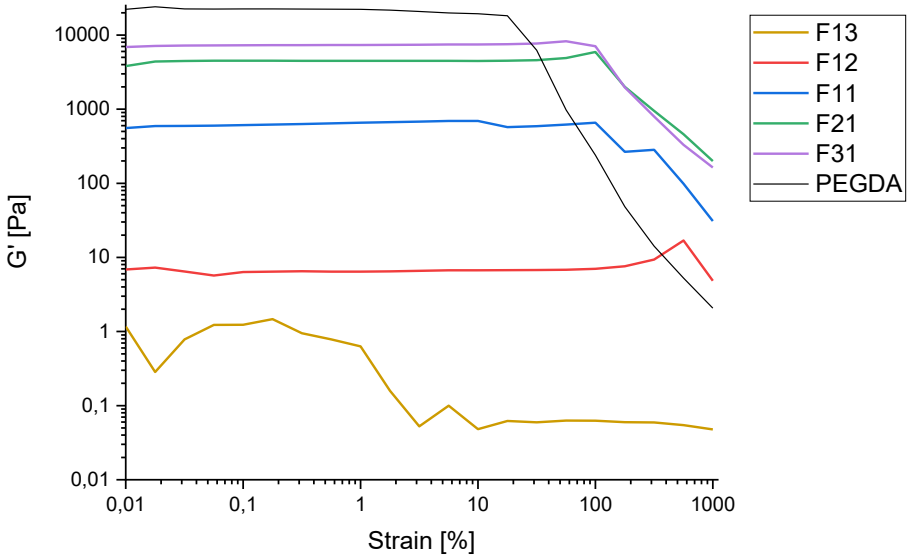

Figure 46 Amplitude sweep test of PEGMEMA-based formulations.

Putting aside the formulation F13 that did not polymerize, all the others showed a PEGMEMA-dependent mechanical behaviour. Indeed, the increasing amount of PEGMEMA over PEGDA translated into the formation of progressively softer and more elastic hydrogels, that can be noticed by the drop of the storage modulus G' and the elongation of the LVE region. However, there is no evidence of a proportional trend.

To better understand the polymerization kinetics, a **photorheological time sweep test** has been run, setting once again the amplitude sweep at 1% according to the previous test.

Figure 47 displays the polymerization trends of the five formulations and compares them to the PEGDA-based one.

Overall, hydrogels' mechanical resistance dropped and gel point shifted onward with the increasing number of PEGMEMA molecules.

As expected from the previous test, there were too many monofunctional monomers in F13 that the network did not manage to form, thus this formulation was excluded from the choice.

The formulation F12 was left behind too because, even if it polymerized, it took too long (about 80 seconds) to appreciate the irradiation effects on the crosslinking reaction. Furthermore, the final hydrogel was mechanically too weak and samples would have risked to break easily.

Among the remaining formulations, **F21** seemed to be the most appropriate one. The storage modulus of the solid hydrogel was approximately ten times lower that the PEGDA-

based one, meaning that meshes are bigger enough to guarantee a more evident swelling behavior, and the UV exposure time was sufficiently brief preventing DNA from UV damage once inserted into the resin.

Therefore, it was the only formulation on which the subsequent experiments were conducted and, for this reason, it will be referred to as **PEGMEMA-based resin** from now on.

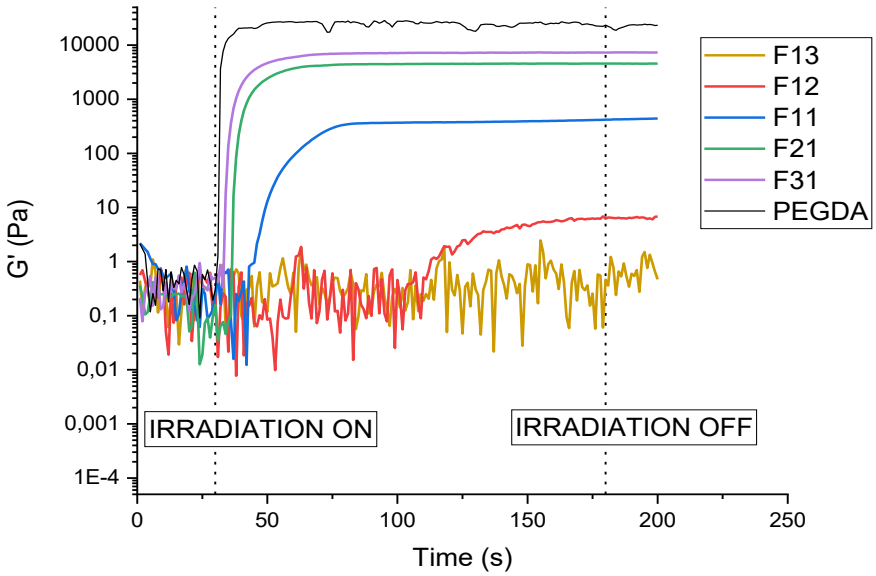

Figure 47 Time sweep test of PEGMEMA-based formulations.

4.2.2 3D printing

Rheological tests revealed that the PEGMEMA-based resin was not very dissimilar to the PEGDA-based one, hence printing parameters were firstly retrieved from the former ones and then modified, raising the UV exposure time and the light intensity of the UV source. The advanced parameter “Fill exposure” was manipulated to avoid the unintended effect of the sample splattering due to the leak of a light absorber.

After several trials, parameters in Table 12 assured an acceptable resolution of samples with **simple geometry**, with or without DNA.

	Burn-in	**Other layers**
Number of layers	13	till the end
Layer thickness [µm]	15	15
Exposure time [s]	8	6
Light intensity [mW/cm^2]	50	50
Fill Exposure [%]	50	50
Separation velocity [mm/s]	3	3
Approach velocity [mm/s]	3	3

Table 12 Printing parameters of PEGMEMA-based resins - simple CADs

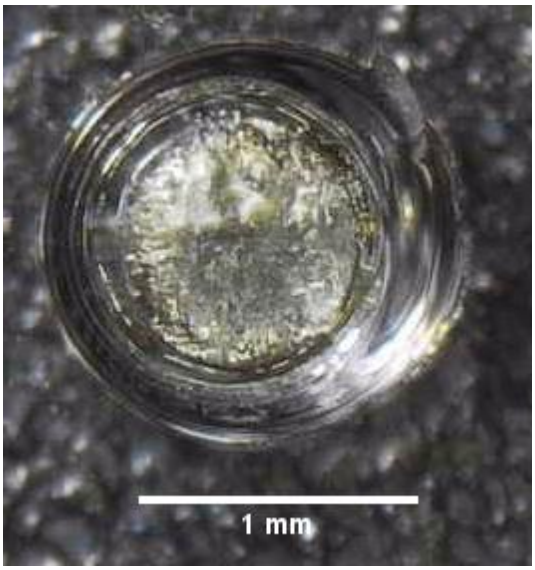

Figure 48 Top view of a printed samples with simple geometry.

In the case of more **complex structures**, instead, to avoid the close-up of holes, the velocity of the platform displacement was changed again as follows:

	Burn-in	Other layers
Number of layers	13	till the end
Layer thickness [µm]	15	15
Exposure time [s]	8	6
Light intensity [mW/cm^2]	50	50
Fill Exposure [%]	50	50
Separation velocity [mm/s]	1	1
Approach velocity [mm/s]	1	1
Wait time (after separation) [s]	2	2

Table 13 Printing parameters of PEGMEMA-based resins - complex CADs

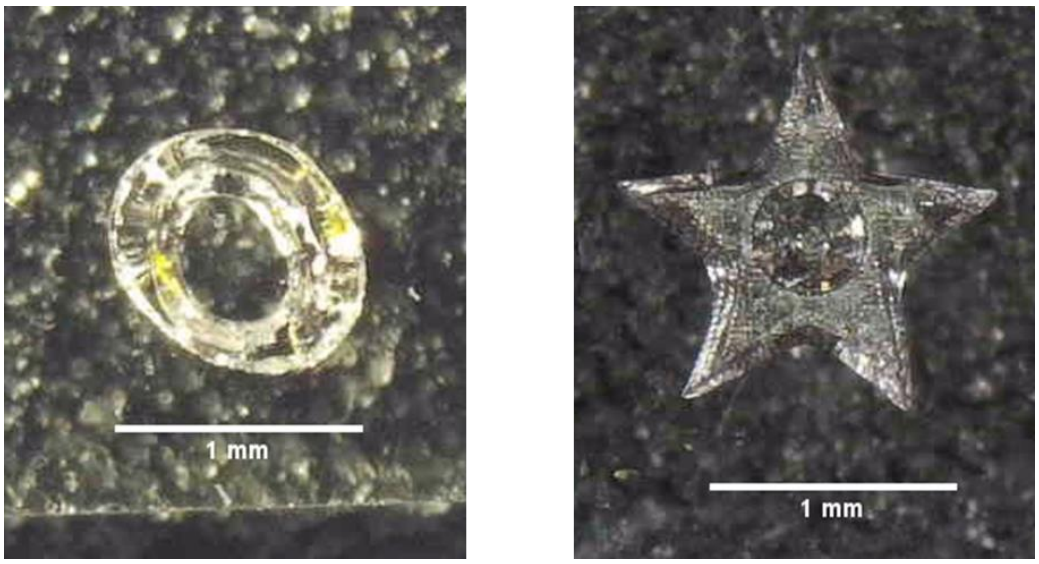

Figure 49 Top view of printed samples with complex geometries.

Considering the extraordinary ability of 3D printers of producing tiny hydrogels with good resolution, its performances have been further challenged by the implementation of a **multi-material printing**. The idea was to design a CAD with two stacked cylinders, previously described in paragraph 4.1.2.1, in which one was DNA-based, while the other DNA-free.

Thus, since DNA does not alter the printing parameters, the 3D printer was instructed to repeat the same sequence of parameters, namely the burn-in and the next layers, a second time after the printing of the first cylinder.

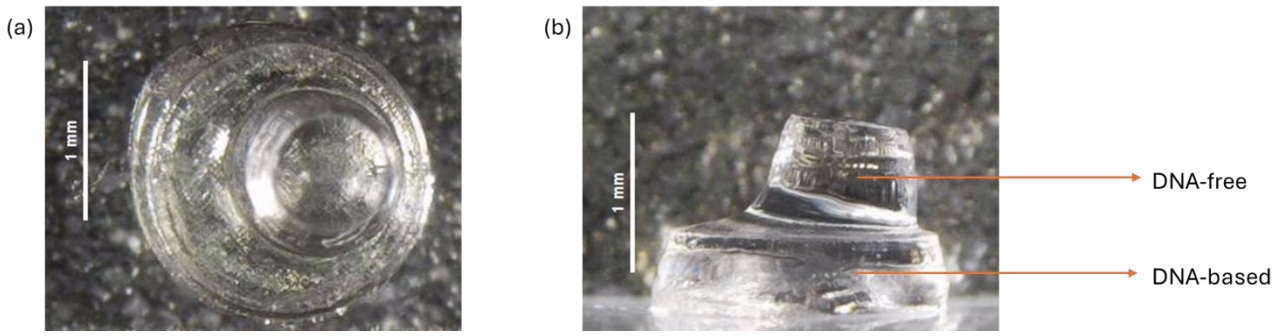

Figure 50 Top view (a) and side view (b) of the multi-material sample.

From Figure 50 it can be noticed that the final sample is not composed by two coaxial cylinders, contrary to what was expected from the CAD. The platform was removed from its allocation after the printing of the first cylinder to be thoroughly cleaned to avoid contamination between the two resins. That's why, after the replacement, its absolute position slightly changed and affected the coordinated of the second cylinder.

4.2.3 DNA-driven expansion

4.2.3.1 Simple-shaped hydrogels

As PEGMEMA has been added to the formulation to influence the swelling ratio, predictably it has influenced the **swelling kinetics** too. Consequently, the swelling protocol has been slightly modified. Equilibrium was not reached in 24 hours but in 48, so samples have been immersed in TAE/Mg^{2+} for **two days** and then, as previously, in the expansion buffer for four days.

In analogy to PEGDA-based hydrogels, the DNA-driven expansion was evaluated only by measuring the surface variation. During the first phase, both DNA and control expanded of the same proportion: DNA's SSR was 52,39 ± 32,73 %, while control's one 54,12 ± 30,71%.

Then, during the second phase, only DNA further expanded by 12,92 ± 7,00 %, whereas control faintly lowered by – 4,18 ± 7,16 %.

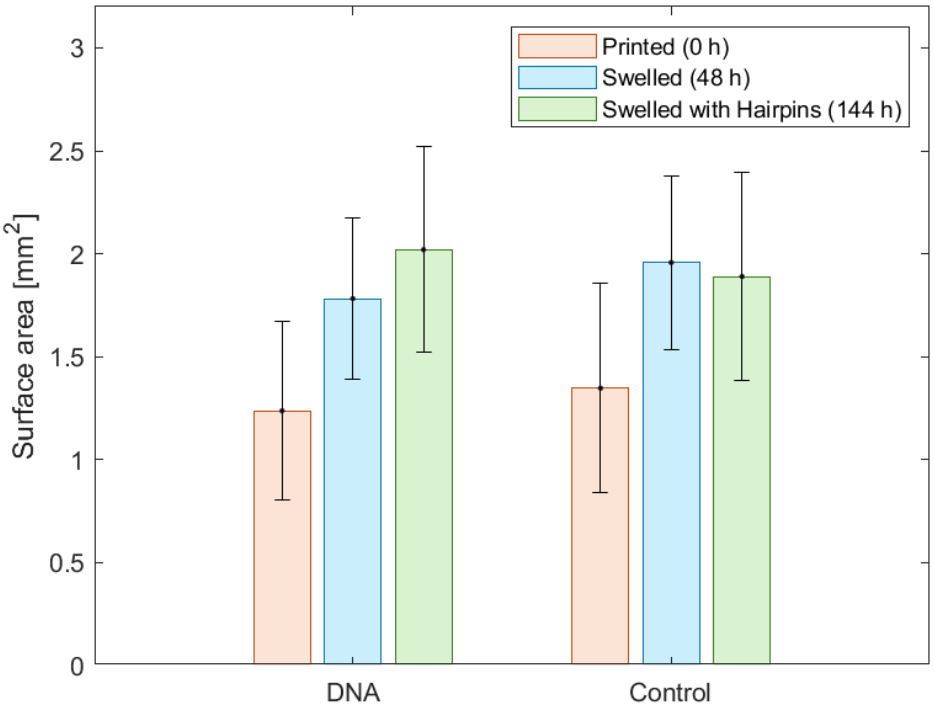

Figure 51 Surface area of PEGMEMA-based samples during the three steps of the DNA-driven expansion.

Standard deviation was roughly significant during this essay too, so the statistical t-test was performed once again, preceded by the Shapiro-Wilks one.

This last confirmed that data followed the normal law, as in Table 14, and allowed to proceed with the second one, whose results are expressed in Table 15.

		p-value	Kurtosis	Result
DNA	1st phase	0,70	2,26	Normal distribution
	2nd phase	0,36	2,54	Normal distribution
Control	1st phase	0,93	2,24	Normal distribution
	2nd phase	0,18	2,64	Normal distribution

Table 14 Shapiro-Wilks results for PEGMEMA-based samples.

		p-value	Result
DNA	1st phase	0,00	Different mean
	2nd phase	0,01	**Different mean**
Control	1st phase	0,00	Different mean
	2nd phase	0,27	**Same mean**

Table 15 Student test for PEGMEMA-based samples.

Comparing data from this experience to the ones obtained above, some reflections can be developed. The addition of PEGMEMA factually allowed the hydrogel surface to expand more than twice, from 20% to 50%, during the first step, while perhaps had no effect on the second phase. In fact, DNA surface increased approximately of the same quantity, while control maintained its dimensions or steadily decreased.
However, the actual distinction between PEGDA and PEGMEMA comes from statistics: while DNA-driven expansion for the DNA-based samples in the first experience had a 92% confidence interval, so that the null hypothesis cannot be rejected; on the other hand, the same PEGMEMA-based samples had a 99% confidence interval assuring the success of the DNA-driven expansion reaction. In fact, the acceptance of the null hypothesis in PEGDA-based samples had very weak basis, since the confident level was too close to the 95% threshold.

All in all, the **hybridization chain reaction process** is finally **achieved** and statistically supported.

4.2.3.2 Complex-shaped hydrogels

Regarding hydrogels with complex geometries and the multi-material one, DNA-driven expansion has been estimated only **visually** for two main reasons: samples were too frangible due to the presence of a central hole that has reduced their mechanical resistance and surface edges were hard to manually detect because of the splattering of samples that did not make it easy to identify a single plane. However, samples had the following appearance after each step:

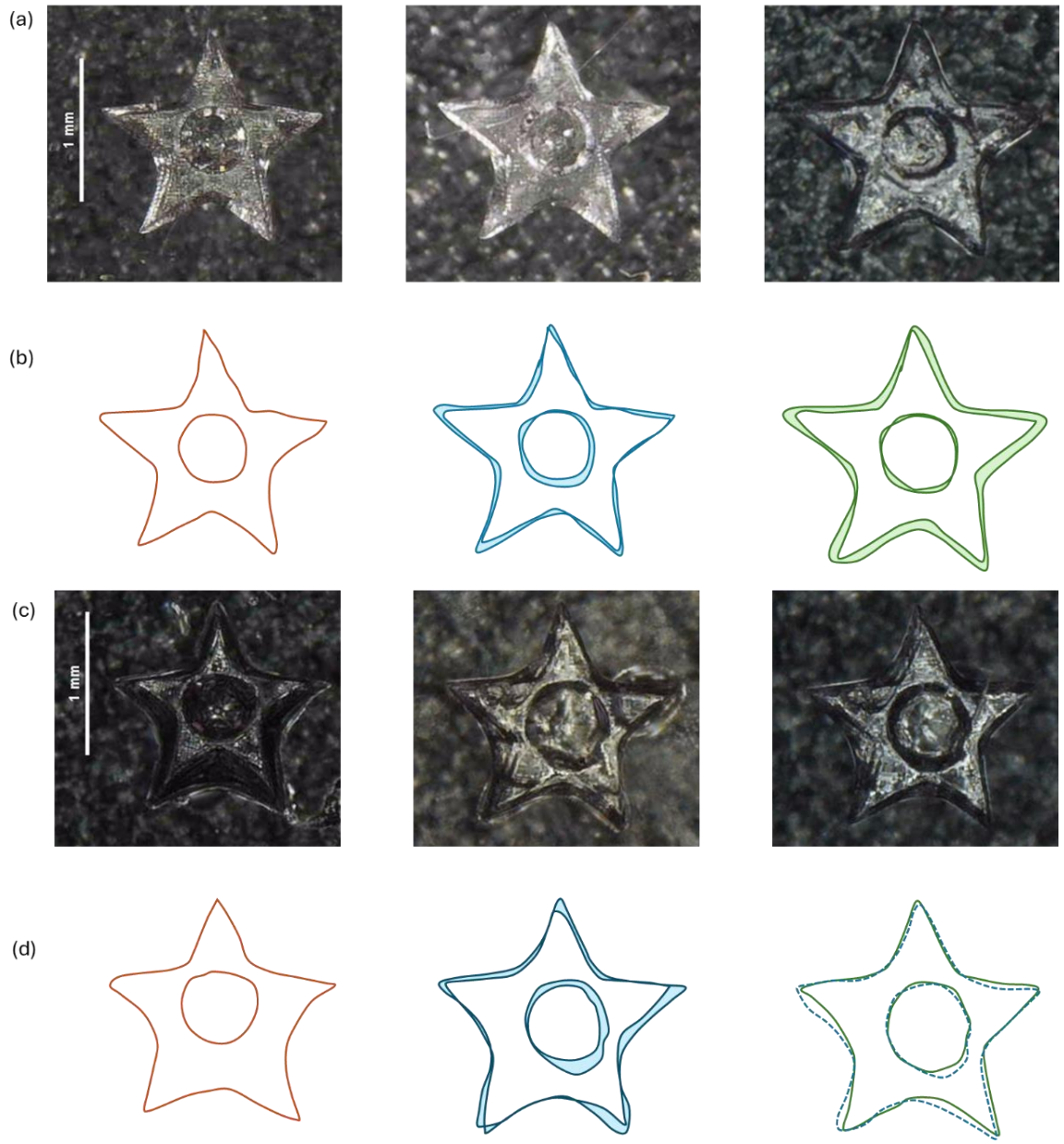

Figure 52 The three phase of DNA-driven expansion process for complex DNA (a) and control (c) samples, with graphical representation of the expansion (respectively (b) and (d)).

The multi-material hydrogel has been swelled too, as follows:

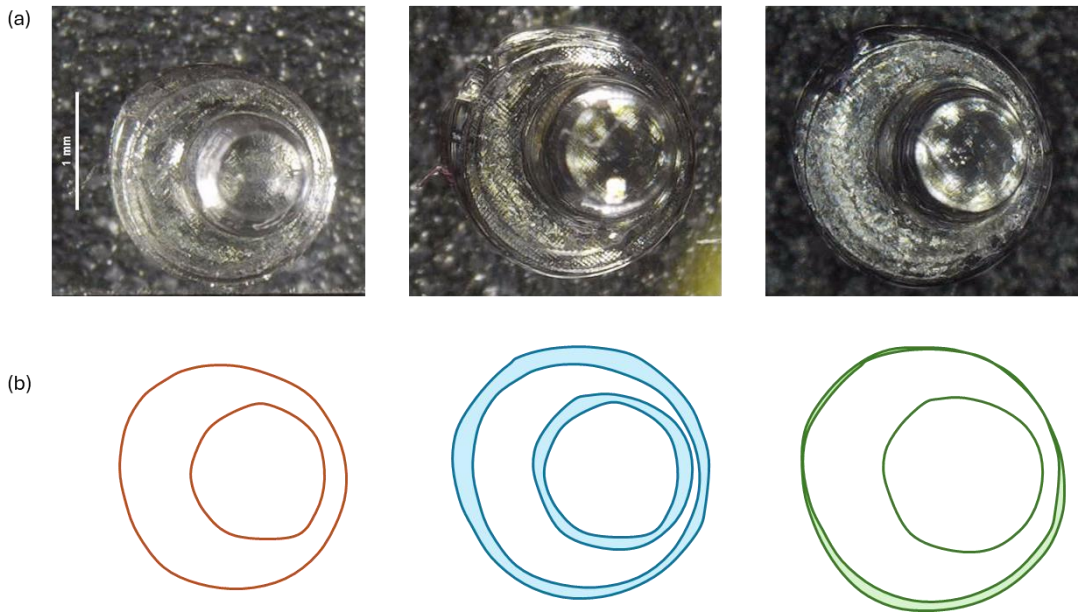

Figure 53 The three phase of DNA-driven expansion process for a multi-material sample (a), with graphical representation of the expansion (b).

Despite the difficulty in distinguishing boundaries between the two layers, it can be noticed that the DNA-based layer managed to expand in the expansion buffer, while the other one stabilized its dimensions.

This is a valuable achievement in the perspective of engineering **more complex structures**, e.g. soft robots, which can not only expand but also fold (and unfold) or move, thanks to the contribution apported by the 3D printing technology.

4.2.4 Specificity of DNA-driven expansion

The predefined aim of this thesis work to validate the **hybridization chain reaction process** has **successfully** been **accomplished** through the forementioned experiences. Consequently, some more in-deep analyses have been carried out with focus on the nature of oligonucleotides. From scientifical literature (92), only specific sequences of nitrogenous bases can be stimulated by the HCR cascading mechanism. This is the reason why they should be designed in advance and synthetically produced in laboratory with advanced techniques, contrary to a simpler DNA extraction from cells. Hence, during this thesis work it was intended to give an answer to the doubtful **specific nature** of this process.

3D-printed samples and the experiment set-up were the same as for previous tests on PEGMEMA-based samples; the only difference was the DNA-driven expansion buffer which contained 40 μM of **not complementary hairpins**.

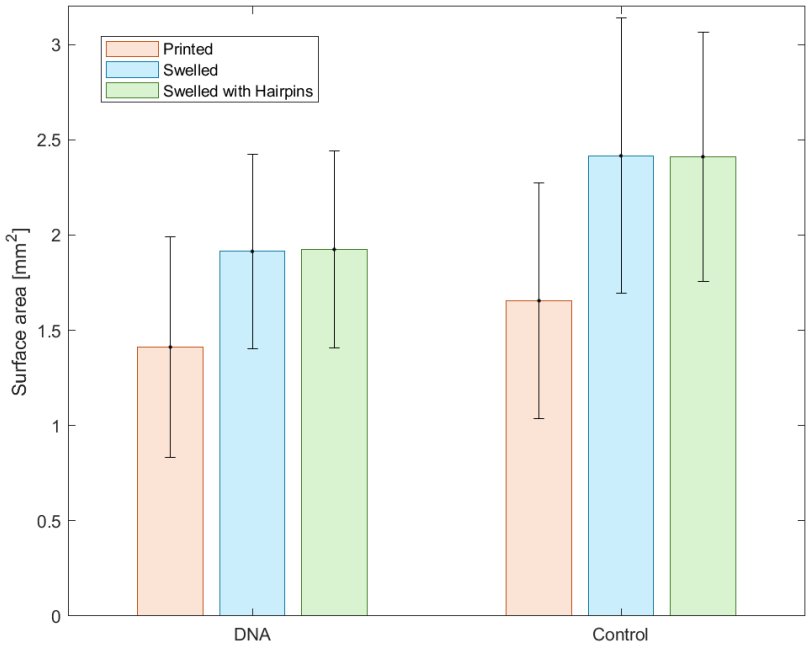

Figure 54 Surface area of PEGMEMA-based samples during the three steps of the DNA-driven expansion in a buffer with not complementary hairpins.

The first phase showed values consistent with those previously observed: DNA expanded by 41,74 ± 19,56 %, while control by 50,66 ± 22,74 %. During the second part of the swelling, instead, expansion was approximately null for both: 0,51 ± 0,76 % for DNA and 0,34 ± 3,50 % for control.

Once again statistical tests confirmed the consistency of results, as follows:

		p-value	Kurtosis	Result
DNA	1st phase	0,59	2,45	Normal distribution
	2nd phase	0,84	2,21	Normal distribution
Control	1st phase	0,43	1,50	Normal distribution
	2nd phase	0,94	2,22	Normal distribution

Table 16 Shapiro-Wilks results for PEGMEMA-based samples (verification of specificity).

		p-value	Result
DNA	1st phase	0,00	Different mean
	2nd phase	0,10	**Same mean**
Control	1st phase	0,00	Different mean
	2nd phase	0,90	**Same mean**

Table 17 Student test for PEGMEMA-based samples (verification of specificity).

In light of these findings, it can be stated that the acrydite dsDNA linked to the hydrogel does not interact with not complementary ssDNA in the expansion buffer, thus assuring the **high specificity** of the HCR process.

5 CONCLUSIONS

All in all, the purpose of this work was to design a hybrid DNA-based hydrogel responsive to the hybridization chain reaction process, aiming to appreciate a macroscopical expansion through the addition of nucleic acidic fuel. DLP 3D printing was selected as fabrication method because of the possibility of printing elaborate structures and, as far as we know, there are few evidence in scientific literature of the employment of this process for DNA-based hydrogels.

In the first chapiter, the **hydrogel** definition has been provided, besides the methods to produce them according to their classification. Then, a small overview of the main applications in the biomedical field was discussed. Eventually, DNA-based hydrogels have been investigated though a wide digression on their structure and potential ways to trigger them.

The second chapiter treated, instead, the history of the **additive manufacturing** and its benefits over traditional fabrication techniques. All the main additive manufacturing methods have been briefly explained, even if only the vat polymerization has been discussed with greater level of detail. This is because the method adopted during this thesis work belongs to this category. At the end of this part, examples of additive manufacturing applications in diverse engineering fields have been shown with focus on the biomedical sector and, with greater detail, on hydrogels.

The third chapiter regarded the exhaustive clarification of the **materials** employed and the explication of the adopted **methodologies** to produce the resin formulation, characterize the material and evaluate the DNA-driven expansion. While the fourth part discussed the **experimental results**.

Acrydite-modified DNA was crosslinked to **PEGDA 700 MW** molecules during the photopolymerization to form final hydrogels. Simple and complex geometries have been successfully achieved thanks to the DLP printer, inspiring the future creation of more structured gels with specific functionalities.

Printed hydrogels underwent the DNA-driven expansion by the performance of a double-stage process: samples were firstly immersed into a simple water-based ionic solution to reach the swelling equilibrium and, only then, translated into the **expansion buffer** containing DNA hairpins, namely the nucleic acidic fuel. DNA-based hydrogels slightly

further expanded during the second phase too, while control DNA-free hydrogels did not. However, this was not statistically supported, therefore another strategy was tented.
PEGMEMA 950 MW was added to the resin formulation in a well-defined molar ratio with PEGDA, aiming to increase the dimension of the polymeric meshes and, hopefully, better appreciate the DNA-driven expansion.
These hydrogels were printed with slightly less accuracy than PEGDA ones, but they were still able to obtain complex geometries.
Discussing about the DNA-driven expansion, PEGMEMA had an effect on the first phase of the process, but it was not evident on the second one, resulting in a percentage of further expansion similar to PEGDA-based hydrogels.
This time, data were statistically supported so the HCR process was successfully verified.

Finally, since DNA is added to hydrogels to provide high specific and reversible response to stimuli, **specificity** was tested. Hydrogels were immersed in a control buffer containing not complementary hairpins and the outcome was noteworthy because they did not expand, confirming the hypothesis.

A protocol for the verification of **reversibility** has not been tested yet, and it is leaved for future developments.

Analogously, some more future perspectives coming from this work's limitations should be considered.
DNA can be damaged by UV light, thus maybe the formulation can be modified in order to try DLP printing within the **visible spectrum** (at least at the wavelength of 405 nm).).
Also, other polymeric precursors can be tested, which may enhance the effect of DNA expansion.

Then, due to the frangibility of hydrogels only the surface area expansion has been evaluated by a manual procedure. A protocol to analyze the **volumetric variation** of samples should be developed and, to overcome the errors due to the manual analysis, an **artificial intelligence** can be trained to automatically recognize surfaces.

Lastly, in a bigger picture, this material can be modified to serve as a **soft robot** component, e.g. an actuator, or as a **biosensor** to detect nucleic acids leaved by living organisms. This can open new, unexplored perspective, especially in the field of hybrid synthetic/DNA materials and devices.

6 ACKNOWLEDGEMENTS

First and foremost, I would like to express my heartfelt thanks to distinguished Professor Ignazio Roppolo and Professor Francesca Frascella for your support and guidance throughout this thesis work.
I would like to thank Eng. Francesco Schimmenti for your incommensurable patience and tremendous help for the entire duration of this research work and Doctor Désirée Baruffaldi for teaching me a lot of skills and knowledge and answering my questions with continuous patience.

Secondly, I would also extend my gratitude to everyone I met in laboratory and with who I shared my days lately, PhD and undergraduate students. It was a pleasure to work with you all and to provide mutual encouragement and critical feedback.

Then, I would like to thank my family who supported me throughout these years.
Thank you, Nathan, for offering me your endless love and outstanding support in life and in mind. Thanks for always being there to encourage me. I am looking forward to sharing my future with you.
Thanks to my adorable aunt, Zia Gisa, for always believing in me and constantly having my back. If I am here, at the end of this journey, it is certainly thanks to you and to a bit of luck that led you to discover this academic path.
I would like to extend my gratitude to mum and dad for your love and sacrifices and to my big little brother for always finding new ways to challenge me and to make me understand in which extent I am strong and brave.
Thank you, Nonno Giacomo and Nonna Giacoma, for your constant support and your prayers to Saint Antonio. Even though we are far apart, you never stop making me feel close to you. I love you.

Finally, I sincerely thank my international friends, Maria and José, for having included me in your life. Thank you for endless conversations in which we share our fears, emotions, dreams and a bit of gossip, too. Since I first met you, you have made my life much happier and lighter. I can’t wait to see you again.
Last but not least, thank you, Professor Messina, for introducing me to science and for always having supported me in pursuing my passions.

7 LIST OF ABBREVIATIONS

AM: additive manufacturing

CAD: computer-aided design

CAL: computed axial lithography

CLIP: continuous liquid interface production

CNC: computerized numerical control

DIW: direct ink writing

DLP: digital light processing

DMD: digital micromirror device

DNA: deoxyribonucleic acid

dsDNA: double-stranded DNA

EBM: electron beam melting

FDM: fused deposition modeling

FFF: fused filament fabrication

H_2O^{N-}: nuclease-free distilled water

H-bonds: hydrogel bonds

IRGACURE 2959 or I2959: 2-hydroxy-1-[4-(2-hydroxyethoxy) phenyl]-2-methyl-1-propanone

LAP: lithium phenyl-2,4,6-trimethylbenzoylphospinate

LVE: linear viscoelastic (region)

MW: molecular weight

PAA: polyacrylamide

PCL: polycaprolactone

PEG: polyethylene glycol

PEGDA: polyethylene glycol diacrylate

PEGMEMA: polyethylene glycol methyl ether methacrylate

PI: photo-initiator

PLA: polylactic acid

PU: polyurethane

ROI: region of interest

SLA: stereolithography

μSLA: micro-stereolithography

SLM: selective laser melting

SLS: selective laser sintering

ssDNA: single-stranded DNA

SSR: surface swelling ratio

STL: standard tessellation language

TAE: tris acetate-EDTA buffer

TAE/Mg^{2+}: tris acetate-EDTA buffer with magnesium chloride

TPO: diphenyl (2,4,6-trimethylbenzoyl) phosphine oxide

TPO-SDS: water-soluble TPO based nanoparticle

T-test: Student test

UAM: ultrasonic additive manufacturing

UV: ultraviolet (light)

VP: vat polymerization

8 REFERENCES

1. Buwalda SJ, Boere KWM, Dijkstra PJ, Feijen J, Vermonden T, Hennink WE. Hydrogels in a historical perspective: From simple networks to smart materials. J Control Release. 2014 Sep 28;190:254–73.
2. Alemán J V, Chadwick A V, He J, Hess M, Horie K, Jones RG, et al. Definitions of terms relating to the structure and processing of sols, gels, networks, and inorganic-organic hybrid materials (IUPAC Recommendations 2007). 2007;79(10):1801–29. Available from: https://doi.org/10.1351/pac200779101801
3. Karlsson S, Albertsson A. Biodegradable polymers and environmental interaction. Polym Eng Sci [Internet]. 1998;38(8):1251–3. Available from: https://4spepublications.onlinelibrary.wiley.com/doi/abs/10.1002/pen.10294
4. Bhatia S. Natural Polymers vs Synthetic Polymer. In: Natural Polymer Drug Delivery Systems: Nanoparticles, Plants, and Algae [Internet]. Cham: Springer International Publishing; 2016. p. 95–118. Available from: https://doi.org/10.1007/978-3-319-41129-3_3
5. Zhang Z, Ortiz O, Goyal R, Kohn J. Chapter 23 - Biodegradable Polymers. In: Lanza R, Langer R, Vacanti J, editors. Principles of Tissue Engineering (Fourth Edition) [Internet]. Fourth Edition. Boston: Academic Press; 2014. p. 441–73. Available from: https://www.sciencedirect.com/science/article/pii/B9780123983589000239
6. Ingavle GC, Gehrke SH, Detamore MS. The bioactivity of agarose–PEGDA interpenetrating network hydrogels with covalently immobilized RGD peptides and physically entrapped aggrecan. Biomaterials [Internet]. 2014;35(11):3558–70. Available from: https://www.sciencedirect.com/science/article/pii/S0142961214000039
7. Maitra J, Shukla V. Cross-linking in hydrogels - a review. Am J Polym Sci. 2014 Jun;4:25–31.
8. Gennen S, Grignard B, Thomassin J-M, Gilbert B, Vertruyen B, Jerome C, et al. Polyhydroxyurethane hydrogels: Synthesis and characterizations. Eur Polym J [Internet]. 2016;84:849–62. Available from: https://www.sciencedirect.com/science/article/pii/S0014305716307650
9. McKeen LW. 3 - Introduction to Plastics and Polymers. In: McKeen LW, editor. Fatigue and Tribological Properties of Plastics and Elastomers (Third Edition) [Internet]. Third Edition. William Andrew Publishing; 2016. p. 45–64. Available from: https://www.sciencedirect.com/science/article/pii/B9780323442015000034
10. Hennink WE, van Nostrum CF. Novel crosslinking methods to design hydrogels. Adv Drug Deliv Rev [Internet]. 2002;54(1):13–36. Available from: https://www.sciencedirect.com/science/article/pii/S0169409X0100240X
11. Sperinde J, Griffith LG. Synthesis and Characterization of Enzymatically-Cross-Linked Poly(ethylene glycol) Hydrogels. Macromolecules [Internet]. 1997;30:5255–64. Available from: https://api.semanticscholar.org/CorpusID:96008605

12. Westhaus E, Messersmith PB. Triggered release of calcium from lipid vesicles: a bioinspired strategy for rapid gelation of polysaccharide and protein hydrogels. Biomaterials [Internet]. 2001;22(5):453–62. Available from: https://www.sciencedirect.com/science/article/pii/S0142961200002003

13. Abasalizadeh F, Moghaddam SV, Alizadeh E, akbari E, Kashani E, Fazljou SMB, et al. Alginate-based hydrogels as drug delivery vehicles in cancer treatment and their applications in wound dressing and 3D bioprinting. J Biol Eng [Internet]. 2020;14(1):8. Available from: https://doi.org/10.1186/s13036-020-0227-7

14. Watanabe T, Ohtsuka A, Murase N, Barth P, Gersonde K. NMR studies on water and polymer diffusion in dextran gels. Influence of potassium ions on microstructure formation and gelation mechanism. Magn Reson Med [Internet]. 1996;35(5):697–705. Available from: https://onlinelibrary.wiley.com/doi/abs/10.1002/mrm.1910350511

15. Yu H, Xiao Q, Qi G, Chen F, Tu B, Zhang S, et al. A Hydrogen Bonds-Crosslinked Hydrogels With Self-Healing and Adhesive Properties for Hemostatic. Front Bioeng Biotechnol [Internet]. 2022;10. Available from: https://www.frontiersin.org/journals/bioengineering-and-biotechnology/articles/10.3389/fbioe.2022.855013

16. Cheng E, Xing Y, Chen P, Yang Y, Sun Y, Zhou D, et al. A pH-Triggered, Fast-Responding DNA Hydrogel. Angew Chemie Int Ed [Internet]. 2009;48(41):7660–3. Available from: https://onlinelibrary.wiley.com/doi/abs/10.1002/anie.200902538

17. Yokoyama F, Masada I, Shimamura K, Ikawa T, Monobe K. Morphology and structure of highly elastic poly(vinyl alcohol) hydrogel prepared by repeated freezing-and-melting. Colloid Polym Sci [Internet]. 1986;264:595–601. Available from: https://api.semanticscholar.org/CorpusID:97085321

18. Yang C, Suo Z. Hydrogel ionotronics. Nat Rev Mater [Internet]. 2018;3(6):125–42. Available from: https://doi.org/10.1038/s41578-018-0018-7

19. Caddeo S, Boffito M, Sartori S. Tissue Engineering Approaches in the Design of Healthy and Pathological In Vitro Tissue Models. Front Bioeng Biotechnol [Internet]. 2017;5. Available from: https://www.frontiersin.org/articles/10.3389/fbioe.2017.00040

20. Parente ME, Ochoa Andrade A, Ares G, Russo F, Jiménez-Kairuz Á. Bioadhesive hydrogels for cosmetic applications. Int J Cosmet Sci [Internet]. 2015;37(5):511–8. Available from: https://onlinelibrary.wiley.com/doi/abs/10.1111/ics.12227

21. Musgrave CSA, Fang F. Contact Lens Materials: A Materials Science Perspective. Materials (Basel) [Internet]. 2019;12(2). Available from: https://www.mdpi.com/1996-1944/12/2/261

22. Aswathy SH, Narendrakumar U, Manjubala I. Commercial hydrogels for biomedical applications. Heliyon [Internet]. 2020;6(4):e03719. Available from: https://www.sciencedirect.com/science/article/pii/S2405844020305648

23. Lee Y, Song WJ, Sun J-Y. Hydrogel soft robotics. Mater Today Phys [Internet]. 2020;15:100258. Available from: https://www.sciencedirect.com/science/article/pii/S2542529320300821

24. Sun J-Y, Zhao X, Illeperuma WRK, Chaudhuri O, Oh KH, Mooney DJ, et al. Highly stretchable and tough hydrogels. Nature [Internet]. 2012;489(7414):133–6. Available from: https://doi.org/10.1038/nature11409

25. Zheng J, Xiao P, Le X, Lu W, Théato P, Ma C, et al. Mimosa inspired bilayer hydrogel actuator functioning in multi-environments. J Mater Chem C [Internet]. 2018;6(6):1320–7. Available from: http://dx.doi.org/10.1039/C7TC04879C

26. WATSON JD, CRICK FHC. Molecular Structure of Nucleic Acids: A Structure for Deoxyribose Nucleic Acid. Nature [Internet]. 1953;171(4356):737–8. Available from: https://doi.org/10.1038/171737a0

27. Bates SA. DEOXYRIBONUCLEIC ACID (DNA) [Internet]. 2024. Available from: https://www.genome.gov/genetics-glossary/Deoxyribonucleic-Acid

28. Matos-Rodrigues G, Hisey JA, Nussenzweig A, Mirkin SM. Detection of alternative DNA structures and its implications for human disease. Mol Cell [Internet]. 2023 Oct 19;83(20):3622–41. Available from: https://doi.org/10.1016/j.molcel.2023.08.018

29. Kosiol N, Juranek S, Brossart P, Heine A, Paeschke K. G-quadruplexes: a promising target for cancer therapy. Mol Cancer [Internet]. 2021;20(1):40. Available from: https://doi.org/10.1186/s12943-021-01328-4

30. Luo X, Zhang J, Gao Y, Pan W, Yang Y, Li X, et al. Emerging roles of i-motif in gene expression and disease treatment. Front Pharmacol [Internet]. 2023;14. Available from: https://www.frontiersin.org/journals/pharmacology/articles/10.3389/fphar.2023.1136251

31. Catuogno S, Esposito CL. Aptamer Cell-Based Selection: Overview and Advances. Biomedicines [Internet]. 2017;5(3). Available from: https://www.mdpi.com/2227-9059/5/3/49

32. LubioScience. Aptamers [Internet]. 2023 [cited 2024 Jul 3]. Available from: https://www.lubio.ch/blog/aptamers

33. Bayda S, Adeel M, Tuccinardi T, Cordani M, Rizzolio F. The History of Nanoscience and Nanotechnology: From Chemical–Physical Applications to Nanomedicine. Molecules [Internet]. 2020;25(1). Available from: https://www.mdpi.com/1420-3049/25/1/112

34. Agarwal S, Klocke MA, Pungchai PE, Franco E. Dynamic self-assembly of compartmentalized DNA nanotubes. Nat Commun [Internet]. 2021;12(1):3557. Available from: https://doi.org/10.1038/s41467-021-23850-1

35. Adleman LM. Molecular Computation of Solutions to Combinatorial Problems. Science (80-) [Internet]. 1994;266(5187):1021–4. Available from: https://www.science.org/doi/abs/10.1126/science.7973651

36. Orbach R, Willner B, Willner I. Catalytic nucleic acids (DNAzymes) as functional units for logic gates and computing circuits: from basic principles to practical applications. Chem Commun [Internet]. 2015;51(20):4144–60. Available from: http://dx.doi.org/10.1039/C4CC09874A

37. Wang F, Lv H, Li Q, Li J, Zhang X, Shi J, et al. Implementing digital computing with DNA-based switching circuits. Nat Commun [Internet]. 2020;11(1):121. Available from: https://doi.org/10.1038/s41467-019-13980-y

38. Nagahara S, Matsuda T. Hydrogel formation via hybridization of oligonucleotides derivatized in water-soluble vinyl polymers. Polym Gels Networks [Internet]. 1996;4(2):111–27. Available from: https://www.sciencedirect.com/science/article/pii/0966782296000019

39. Lattuada E, Leo M, Caprara D, Salvatori L, Stoppacciaro A, Sciortino F, et al. DNA-GEL, Novel Nanomaterial for Biomedical Applications and Delivery of Bioactive Molecules. Front Pharmacol [Internet]. 2020;11. Available from: https://www.frontiersin.org/journals/pharmacology/articles/10.3389/fphar.2020.01345

40. Hu Y, Xu W. Biomedical DNA hydrogels. Soft Sci. 2022 Jul;2:3.

41. Cangialosi A, Yoon CK, Liu J, Huang Q, Guo J, Nguyen TD, et al. DNA sequence–directed shape change of photopatterned hydrogels via high-degree swelling. Science (80-). 2017;357(6356).

42. Shi J, Shi Z, Dong Y, Wu F, Liu D. Responsive DNA-Based Supramolecular Hydrogels. ACS Appl Bio Mater. 2020 Mar 24;3(5):2827–37.

43. Guo W, Qi X-J, Orbach R, Lu C-H, Freage L, Mironi-Harpaz I, et al. Reversible Ag+-crosslinked DNA hydrogels. Chem Commun [Internet]. 2014;50(31):4065–8. Available from: http://dx.doi.org/10.1039/C3CC49140D

44. Kandatsu D, Cervantes-Salguero K, Kawamata I, Hamada S, Nomura SM, Fujimoto K, et al. Reversible Gel–Sol Transition of a Photo-Responsive DNA Gel. ChemBioChem [Internet]. 2016 Jun 16;17(12):1118–21. Available from: https://doi.org/10.1002/cbic.201600088

45. Shi R, Fern J, Xu W, Jia S, Huang Q, Pahapale G, et al. Multicomponent DNA Polymerization Motor Gels. Small. 2020;16(37).

46. Rahmatullah R, Amiruddin A, Lubis S. EFFECTIVENESS OF CNC TURNING AND CNC MILLING IN MACHINING PROCESS. Int J Econ Technol Soc Sci [Internet]. 2021 Oct 30;2(2):575–83. Available from: https://jurnal.ceredindonesia.or.id/index.php/injects/article/view/610

47. 3D Systems. Our story [Internet]. Available from: https://it.3dsystems.com/our-story

48. ISO/ASTM 52900:2021 Additive manufacturing — General principles — Fundamentals and vocabulary. 2021.

49. Kanishka K, Acherjee B. Revolutionizing manufacturing: A comprehensive overview of additive manufacturing processes, materials, developments, and challenges. J Manuf Process [Internet]. 2023;107:574–619. Available from: https://www.sciencedirect.com/science/article/pii/S1526612523009726

50. Chen Y, Zhou C, Lao J. A layerless additive manufacturing process based on CNC accumulation. Bourell D, Stucker B, editors. Rapid Prototyp J [Internet]. 2011 Jan 1;17(3):218–27. Available from: https://doi.org/10.1108/13552541111124806

51. Mizar Additive. DIFFERENCES BETWEEN ADDITIVE MANUFACTURING AND 3D PRINTING [Internet]. Available from: https://mizaradditive.com/en/differences-between-additive-manufacturing-and-3d-printing/

52. Gokhare V, Raut D, Shinde D. A Review paper on 3D-Printing Aspects and Various Processes Used in the 3D-Printing. Int J Eng Tech Res. 2017 Jun 6;6:953–8.

53. Joharji L, Mishra RB, Alam F, Tytov S, Al-Modaf F, El-Atab N. 4D printing: A detailed review of materials, techniques, and applications. Microelectron Eng [Internet]. 2022;265:111874. Available from: https://www.sciencedirect.com/science/article/pii/S016793172200168X

54. Loughborough University. About Additive Manufacturing - Material Extrusion [Internet]. Available from: https://www.lboro.ac.uk/research/amrg/about/the7categoriesofadditivemanufacturing/materialextrusion/#:~:text=Advantages of the material extrusion,method than using injection moulding.

55. Gülcan O, Günaydın K, Tamer A. The State of the Art of Material Jetting—A Critical Review. Polymers (Basel) [Internet]. 2021;13(16). Available from: https://www.mdpi.com/2073-4360/13/16/2829

56. Ding H, Dong M, Zheng Q, Wu ZL. Digital light processing 3D printing of hydrogels: a minireview. Mol Syst Des Eng [Internet]. 2022;7(9):1017–29. Available from: http://dx.doi.org/10.1039/D2ME00066K

57. Lakkala P, Munnangi SR, Bandari S, Repka M. Additive manufacturing technologies with emphasis on stereolithography 3D printing in pharmaceutical and medical applications: A review. Int J Pharm X [Internet]. 2023;5:100159. Available from: https://www.sciencedirect.com/science/article/pii/S2590156723000038

58. Quan H, Zhang T, Xu H, Luo S, Nie J, Zhu X. Photo-curing 3D printing technique and its challenges. Bioact Mater [Internet]. 2020;5(1):110–5. Available from: https://www.sciencedirect.com/science/article/pii/S2452199X19300714

59. Salas A, Zanatta M, Sans V, Roppolo I. Chemistry in light-induced 3D printing. ChemTexts [Internet]. 2023;9(1):4. Available from: https://doi.org/10.1007/s40828-022-00176-z

60. Juskova P, Ollitrault A, Serra M, Viovy J-L, Malaquin L. Resolution improvement of 3D stereo-lithography through the direct laser trajectory programming: Application to microfluidic deterministic lateral displacement device. Anal Chim Acta [Internet]. 2018;1000:239–47. Available from: https://www.sciencedirect.com/science/article/pii/S0003267017313405

61. Ikuta K, Hirowatari K. Real three dimensional micro fabrication using stereo lithography and metal molding. [1993] Proc IEEE Micro Electro Mech Syst [Internet]. 1993;42–7. Available from: https://api.semanticscholar.org/CorpusID:110913866

62. Xue D, Zhang J, Wang Y, Mei D. Digital Light Processing-Based 3D Printing of Cell-Seeding Hydrogel Scaffolds with Regionally Varied Stiffness. ACS Biomater Sci Eng [Internet]. 2019 Sep 9;5(9):4825–33. Available from: https://doi.org/10.1021/acsbiomaterials.9b00696

63. Tomal W, Ortyl J. Water-Soluble Photoinitiators in Biomedical Applications. Polymers (Basel) [Internet]. 2020;12(5). Available from: https://www.mdpi.com/2073-4360/12/5/1073

64. Hager I, Golonka A, Putanowicz R. 3D Printing of Buildings and Building Components as the Future of Sustainable Construction? Procedia Eng [Internet]. 2016;151:292–9. Available from: https://www.sciencedirect.com/science/article/pii/S1877705816317453

65. Yilmaz B, Al Rashid A, Mou YA, Evis Z, Koç M. Bioprinting: A review of processes, materials and applications. Bioprinting [Internet]. 2021;23:e00148. Available from: https://www.sciencedirect.com/science/article/pii/S240588662100021X

66. Guo N, Leu MC. Additive manufacturing: technology, applications and research needs. Front Mech Eng [Internet]. 2013;8(3):215–43. Available from: https://doi.org/10.1007/s11465-013-0248-8

67. Nassar M. Cytological and chromosomal damages induced by tartrazine and two classes (III and IV) of caramelfood dyes. Eur J Biol Res [Internet]. 2022 Jan;12(1). Available from: https://doi.org/10.5281/zenodo.5831912

68. Ge Q, Chen Z, Cheng J, Zhang B, Zhang Y-F, Li H, et al. 3D printing of highly stretchable hydrogel with diverse UV curable polymers. Sci Adv [Internet]. 2024 Jul 15;7(2):eaba4261. Available from: https://doi.org/10.1126/sciadv.aba4261

69. Yang H, Ji M, Yang M, Shi M, Pan Y, Zhou Y, et al. Fabricating hydrogels to mimic biological tissues of complex shapes and high fatigue resistance. Matter [Internet]. 2021;4(6):1935–46. Available from: https://www.sciencedirect.com/science/article/pii/S2590238521001181

70. Ji Z, Yan C, Yu B, Zhang X, Cai M, Jia X, et al. 3D Printing of Hydrogel Architectures with Complex and Controllable Shape Deformation. Adv Mater Technol [Internet]. 2019 Apr 1;4(4):1800713. Available from: https://doi.org/10.1002/admt.201800713

71. Farrag Y, Ait Eldjoudi D, Farrag M, González-Rodríguez M, Ruiz-Fernández C, Cordero A, et al. Poly(ethylene Glycol) Methyl Ether Methacrylate-Based Injectable Hydrogels: Swelling, Rheological, and In Vitro Biocompatibility Properties with ATDC5 Chondrogenic Lineage. Polymers (Basel) [Internet]. 2023;15(24). Available from: https://www.mdpi.com/2073-4360/15/24/4635

72. Rekowska N, Arbeiter D, Brietzke A, Konasch J, Riess A, Mau R, et al. Biocompatibility and thermodynamic properties of PEGDA and two of its copolymer. In: 2019 41st Annual International Conference of the IEEE Engineering in Medicine and Biology Society (EMBC). 2019. p. 1093–6.

73. Suzanne. Biotech Basics: TAE or TBE [Internet]. 2023. Available from: https://blog.edvotek.com/2023/04/27/biotech-basics-to-tae-or-to-tbe/

74. Driessen RPC, Sitters G, Laurens N, Moolenaar GF, Wuite GJL, Goosen N, et al. Effect of Temperature on the Intrinsic Flexibility of DNA and Its Interaction with Architectural Proteins. Biochemistry [Internet]. 2014 Oct 21;53(41):6430–8. Available from: https://doi.org/10.1021/bi500344j

75. Rico-Pasto M, Ritort F. Temperature-dependent elastic properties of DNA. Biophys Reports [Internet]. 2022;2(3):100067. Available from: https://www.sciencedirect.com/science/article/pii/S2667074722000246

76. Khan Academy. Gel electrophoresis [Internet]. Available from: https://www.khanacademy.org/science/ap-biology/gene-expression-and-regulation/biotechnology/a/gel-electrophoresis

77. Xiao P, Zhang J, and Co. 3D Printing with Light. Xiao P, Zhang J, editors. De Gruyter; 2021.

78. Justin Tom P. UV-Vis Spectroscopy: Principle, Strengths and Limitations and Applications [Internet]. 2021. Available from: https://www.technologynetworks.com/analysis/articles/uv-vis-spectroscopy-principle-strengths-and-limitations-and-applications-349865

79. Anton Paar. Amplitude sweeps [Internet]. Available from: https://wiki.anton-paar.com/en/amplitude-sweeps/

80. Santoliquido O, Camerota F, Ortona A. The influence of topology on DLP 3D printing, debinding and sintering of ceramic periodic architectures designed to replace bulky components. Open Ceram [Internet]. 2021;5:100059. Available from: https://www.sciencedirect.com/science/article/pii/S2666539521000055

81. Yang X, Dargaville BL, Hutmacher DW. Elucidating the Molecular Mechanisms for the Interaction of Water with Polyethylene Glycol-Based Hydrogels: Influence of Ionic Strength and Gel Network Structure. Polymers (Basel) [Internet]. 2021;13(6). Available from: https://www.mdpi.com/2073-4360/13/6/845

82. Cavallo A, Madaghiele M, Masullo U, Lionetto MG, Sannino A. Photo-crosslinked poly(ethylene glycol) diacrylate (PEGDA) hydrogels from low molecular weight prepolymer: Swelling and permeation studies. J Appl Polym Sci [Internet]. 2017;134(2). Available from: https://onlinelibrary.wiley.com/doi/abs/10.1002/app.44380

83. Statistical Solutions. Paired T-Test [Internet]. Available from: https://www.statisticssolutions.com/free-resources/directory-of-statistical-analyses/paired-sample-t-test/#:~:text=The paired sample t-test hypotheses are formally defined below%3A&text=The null hypothesis (H0,d) is equal to zero.&text=The two-tailed alternative hypothesis,is not equal to zero.&text=The upper-tailed alternative hypothesis,d is greater than zero.

84. Henderson AR. Testing experimental data for univariate normality. Clin Chim Acta [Internet]. 2006;366(1):112–29. Available from: https://www.sciencedirect.com/science/article/pii/S0009898105006790

85. Gardner-O'Kearny W. Shapiro-Wilk/Shapiro-Francia Tests [Internet]. 2021. Available from: https://it.mathworks.com/matlabcentral/fileexchange/88778-swft-shapiro-wilk-shapiro-francia-tests

86. Kciuk M, Marciniak B, Mojzych M, Kontek R. Focus on UV-Induced DNA Damage and Repair—Disease Relevance and Protective Strategies. Int J Mol Sci [Internet]. 2020;21(19). Available from: https://www.mdpi.com/1422-0067/21/19/7264

87. Hinczewski C, Corbel S, Chartier T. Ceramic suspensions suitable for stereolithography. J Eur Ceram Soc [Internet]. 1998;18(6):583–90. Available from: https://www.sciencedirect.com/science/article/pii/S0955221997001866

88. Strohmeier L, Frommwald H, Schlögl S. Digital light processing 3D printing of modified liquid isoprene rubber using thiol-click chemistry. RSC Adv [Internet]. 2020;10(40):23607–14. Available from: http://dx.doi.org/10.1039/D0RA04186F

89. Mandelkern M, Elias JG, Eden D, Crothers DM. The dimensions of DNA in solution. J Mol Biol [Internet]. 1981;152(1):153–61. Available from: https://www.sciencedirect.com/science/article/pii/0022283681900991

90. Anindita SN, Conti R, Zauchner D, Paunović N, Qiu W, Buzhor MG, et al. Tough PEG-only hydrogels with complex 3D structure enabled by digital light processing of “all-PEG” resins. Aggregate [Internet]. 2023;4(6):e368. Available from: https://onlinelibrary.wiley.com/doi/abs/10.1002/agt2.368

91. Beamish JA, Zhu J, Kottke-Marchant K, Marchant RE. The effects of monoacrylated poly(ethylene glycol) on the properties of poly(ethylene glycol) diacrylate hydrogels used for tissue engineering. J Biomed Mater Res. 2009 Feb 3;92A(2):441–50.

92. Dirks RM, Pierce NA. Triggered amplification by hybridization chain reaction. Proc Natl Acad Sci [Internet]. 2004;101(43):15275–8. Available from: https://www.pnas.org/doi/abs/10.1073/pnas.0407024101